HHS Public Access

Author manuscript

Cell Rep. Author manuscript; available in PMC 2019 November 05.

Published in final edited form as:

Cell Rep. 2019 July 23; 28(4): 1003–1014.e3. doi:10.1016/j.celrep.2019.06.077.

Cholinergic Transmission at Muscarinic Synapses in the Striatum Is Driven Equally by Cortical and Thalamic Inputs

Aphroditi A. Mamaligas[1,2,3], **Kelsey Barcomb**[1], **Christopher P. Ford**[1,2,4,*]

[1]Department of Pharmacology, University of Colorado School of Medicine, Anschutz Medical Campus, Aurora, CO 80045, USA

[2]Departments of Physiology and Biophysics and Neurosciences, Case Western Reserve University School of Medicine, Cleveland, OH 44106, USA

[3]Present address: Gladstone Institute, UCSF, San Francisco, CA 94158, USA

[4]Lead Contact

SUMMARY

The release of acetylcholine from cholinergic interneurons (ChIs) directly modulates striatal output via muscarinic receptors on medium spiny neurons (MSNs). While thalamic inputs provide strong excitatory input to ChIs, cortical inputs primarily regulate MSN firing. Here, we found that, while thalamic inputs do drive ChI firing, a subset of ChIs responds robustly to stimulation of cortical inputs as well. To examine how input-evoked changes in ChI firing patterns drive acetylcholine release at cholinergic synapses onto MSNs, muscarinic M4-receptor-mediated synaptic events were measured in MSNs overexpressing G-protein gated potassium channels (GIRK2). Stimulation of both cortical and thalamic inputs was sufficient to equally drive muscarinic synaptic events in MSNs, resulting from the broad synaptic innervation of the stimulus-activated ChI population across many MSNs. Taken together, this indicates an underappreciated role for the extensive cholinergic network, in which small populations of ChIs can drive substantial changes in post-synaptic receptor activity across the striatum.

Graphical Abstract

*Correspondence: christopher.ford@ucdenver.edu.

AUTHOR CONTRIBUTIONS

A.A.M. and C.P.F. designed the project. A.A.M. performed experiments, and K.B. assisted with experiments by comparing responding and non-responding ChIs. A.A.M., K.B., and C.P.F. analyzed the data. A.A.M. and C.P.F. wrote the manuscript.

SUPPLEMENTAL INFORMATION

Supplemental Information can be found online at https://doi.org/10.1016/j.celrep.2019.06.077.

DECLARATION OF INTERESTS

The authors declare no competing interests.

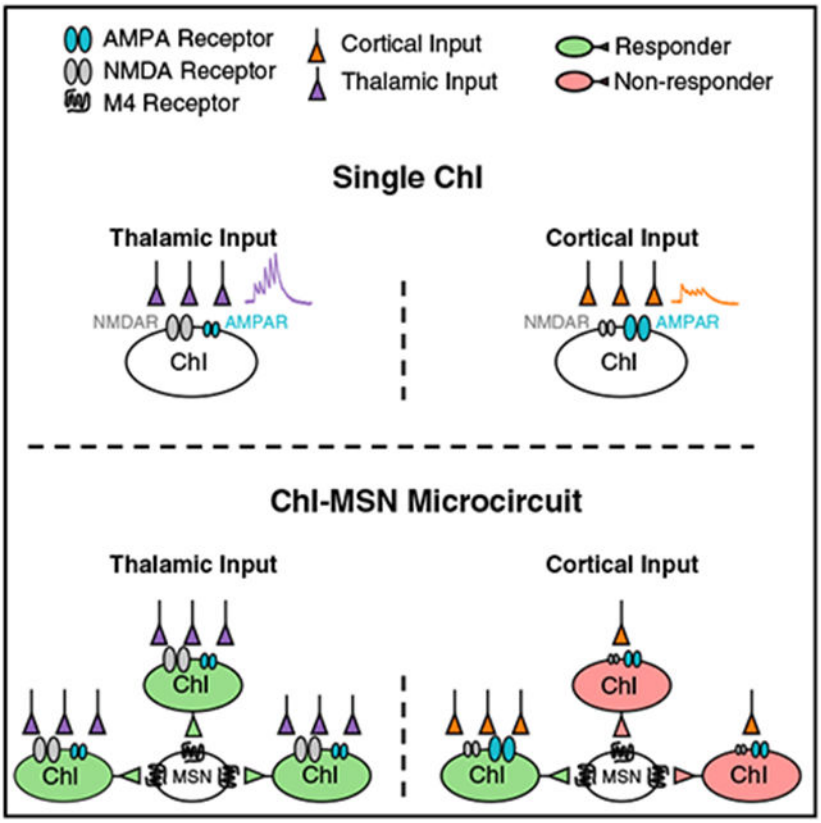

In Brief

Mamaligas et al. find that, while cortical inputs were previously thought to provide weak input to striatal cholinergic interneurons, they can drive firing in a subset of cells. As a result of the broad connectivity of cholinergic cells, cortical and thalamic inputs equally drive synaptic acetylcholine release onto MSNs.

INTRODUCTION

Acetylcholine (ACh) plays an important role in regulating activity in the striatum. While some cholinergic basal forebrain projections target the striatum (Dautan et al., 2014), cholinergic interneurons (ChIs) are the major source of ACh within this region (Lim et al., 2014). Although ChIs comprise only a small percentage of striatal neurons (Kreitzer, 2009), increases in ChI activity can drive striatal-dependent associative behaviors (Bradfield et al., 2013; Stalnaker et al., 2016), while pauses in ChI firing gate associative learning and are sufficient to alleviate Parkinsonian symptoms in rodents (Brown et al., 2012; Maurice et al., 2015). The release of ACh from ChIs modulates multiple cell types within the striatum, including the output cells of the striatum, medium spiny neurons (MSNs). Modulation of MSN activity occurs through presynaptic modulation via both nicotinic ACh receptors (nAChRs) and muscarinic receptors (Cachope et al., 2012; English et al., 2011; Goldberg et al., 2012; Higley et al., 2009; Mamaligas et al., 2016; Nelson et al., 2014; Threlfell et al., 2012), as well as direct modulation of MSNs themselves via muscarinic receptors (Cai and

Ford, 2018; Goldberg et al., 2012; Mamaligas and Ford, 2016). Of the five subtypes of muscarinic receptors, $G_{q/11}$-coupled M1 receptors are expressed on both direct pathway D1-MSNs and indirect pathway D2-MSNs, while $G_{i/o}$-coupled M4-muscarinic receptors are primarily expressed on D1-MSNs (Hersch et al., 1994; Kreitzer, 2009). In D1-MSNs, ChIs make monosynaptic connections with MSNs at M4-muscarinic synapses, with multiple ChIs making independent synaptic connections onto a given MSN (Mamaligas and Ford, 2016). The activation of M4 receptors on MSNs results in G-protein-mediated inhibition of Ca^{2+} channels, as well as decreased collateral activity between MSNs, leading to a decrease in excitability and inhibition of long-term potentiation (Mamaligas and Ford, 2016; Perez-Rosello et al., 2005; Yamamoto et al., 2013).

Although ChIs exhibit endogenous pacemaker activity, firing between 1 and 10 Hz (Bennett and Wilson, 1999; Graybiel et al., 1994), they display stereotyped “burst-pause-burst” firing patterns *in vivo* in response to salient environmental stimuli (Aosaki et al., 1995; Graybiel et al., 1994; Morris et al., 2004). These transient bursts, lasting approximately 50 ms each (Aosaki et al., 1995; Apicella et al., 1997; Morris et al., 2004), are thought to be predominantly generated via excitatory inputs from the intralaminar thalamic nuclei (Ding et al., 2010; Matsumoto et al., 2001; Threlfell et al., 2012). Previous work has determined that input from the parafascicular nucleus of the thalamus (Pf) is both correlated with and necessary for this stereotyped firing pattern *in vivo* (Matsumoto et al., 2001). While the sensorimotor cortex comprises the other predominant excitatory input in the dorsal striatum (Gerfen, 1992), it sends stronger inputs to MSNs than to ChIs (Ding et al., 2008, 2010). Although motor cortex stimulation can increase ChI firing *in vivo* (Doig et al., 2014; Reynolds and Wickens, 2004; Zhang et al., 2018), cortical activity does not correlate strongly with ChI firing patterns, leaving the direct role of cortical inputs on ChI firing unclear (Sharott et al., 2012). Likewise, work from brain slices has shown that while the parafascicular nucleus of the thalamus inputs drive bursts of action potentials in ChIs, the strength of ChI activation following cortical stimulation has been controversial, with some studies reporting small increases in ChI firing, while others have found robust bursting of these cells (Ding et al., 2010; Kosillo et al., 2016). Despite this debate, the difference in the strength of these two inputs is thought to be due to the differing degrees of synaptic facilitation between cortical and thalamic inputs onto ChIs (Aceves Buendia et al., 2019; Ding et al., 2008).

Despite our knowledge of mechanisms underlying input-specific ChI activity, the effect of ACh that may be released onto MSNs in response to these firing patterns remains unclear. While it has been recently shown that cortical inputs can increase the firing of ChIs to drive dopamine release in the striatum (Kosillo et al., 2016), the relative role of cortical and thalamic inputs in driving ACh release onto MSNs has not been addressed. To understand the functional consequences of ChI firing patterns in response to corticostriatal and thalamostriatal stimuli, we used optogenetic activation of excitatory cortical and thalamic inputs to the striatum. We found that thalamic inputs indeed drive ChI firing more effectively than cortical inputs. However, while the firing of the majority of ChIs was unaffected by cortical inputs, some cells had synaptic properties necessary to drive action potentials following cortical stimulation. Despite the majority of ChIs failing to respond to cortical stimulation, both cortical and thalamic inputs equally drove ACh release at muscarinic

synapses onto direct pathway D1-MSNs to a similar extent, likely as a result of the broad innervation of multiple ChIsto each MSN. Overall, our results suggest that the convergence of ChIs at muscarinic synapses allows reliable ACh release onto direct pathway MSNs, even when only a subset of ChIs are activated. Thus, cortical inputs that evoke firing in only a subset of ChIs can broadly drive ACh release in the striatum at muscarinic synapses.

RESULTS

A Subpopulation of ChIs Increases Firing in Response to Cortical Stimulation

To examine the role of excitatory striatal inputs on ChI activity in the dorsolateral striatum, an adeno-associated virus (AAV) encoding a floxed channelrhodopsin (ChR2) and an enhanced yellow fluorescent protein (eYFP) fluorophore (AAV.DIO.ChR2. eYFP) was injected into either the M1 region of the motor cortex or the parafascicular nucleus of the thalamus of CaMKII-Cre heterozygous mice. Three weeks post injection, neurons in both the M1 and the parafascicular nucleus of the thalamus displayed robust YFP expression (Figures 1A and 1B). As noted previously (Hunnicutt et al., 2014, 2016; Smith et al., 2009), fibers originating from the M1 could be seen in the dorsolateral striatum, while thalamic fibers were broadly distributed throughout the striatum (Figures 1A and 1B). We performed whole-cell voltage clamp recordings of ChIs in the dorsolateral striatum (V_h = −80 mV) and stimulated either cortical or thalamic inputs with a single pulse of blue light (2 ms, 470 nm). We recorded ChIs randomly within the center of the dorsolateral striatum for both groups to avoid recording near the cortex when ChR2 was expressed in the motor cortex or near the thalamus when ChR2 was expressed in the parafascicular thalamus. ChIs were distinguished from TH^+ interneurons by their size (~30 μm) and input resistance (79.8 ± 4 MΩ, n = 70 cells). We found that optogenetically evoked, α-amino-3-hydroxy-5-methyl-4-isoxazole-propionic acid (AMPA)-receptor-mediated excitatory post-synaptic currents (EPSCs) were similar in amplitude when evoked from cortical and thalamic terminals (thalamus: −193 ± 70 pA, n = 10; cortex: −211 ± 50 pA, n = 7; p>0.05, Mann-Whitney) (Figures 1C and 1D) and had similar AMPA/N-methyl-D-aspartate (NMDA) ratios (NMDA EPSCs measured at V_h = +40 mV; thalamus: 2.0 ± 0.3, n = 7; cortex: 1.6 ± 0.3, n = 8; p > 0.05, Mann-Whitney) (Figures 1C and 1E). Thus, there were no differences in the magnitudes of transmission at these two synapses for a single stimulus.

Previous work examining excitatory post-synaptic potentials (EPSPs) found that thalamic inputs facilitate, allowing for bursts of thalamic excitation to strongly drive ChI firing (Aceves Buendia et al., 2019; Ding et al., 2010). In contrast, cortical inputs depress, resulting in cortical inputs only weakly driving ChI firing (Ding et al., 2010; but see Kosillo et al., 2016). To examine this, we performed whole-cell current clamp recordings of ChIs and recorded EPSPs in response to a burst of stimuli, which has been used in these previous studies (5 stimuli, 50 Hz, 2 ms each). Although there was no overall difference in the amplitude of EPSPs on the first pulse (thalamus: 2.0 ± 0.5 mV, n = 14; cortex: 2.4 ± 0.9 mV, n = 15; p > 0.05, Mann-Whitney) (Figures 1F and 1H), thalamic inputs indeed displayed robust facilitation, whereas cortical inputs depressed (thalamus 5th pulse/1st pulse: 2.1 ± 0.3, n = 10; cortex 5th pulse/1st pulse: 0.92 ± 0.07, n = 10; p < 0.001, Mann-Whitney; across pulses p < 0.001, 2-way ANOVA) (Figures 1F and 1G).

Next, we examined the same question using cell-attached recordings of ChIs, allowing for observation of intrinsic firing patterns without disturbing the intracellular environment. Similar to previous findings, thalamic excitation (5 pulses, 50 Hz) increased the firing probability of all ChIs recorded during the 100-ms window following the stimulus compared to baseline (baseline probability: 0.24 ± 0.06; stimulus probability: 0.77 ± 0.05; n = 13, $p < 0.001$, Wilcoxon matched pair signed rank) (Figures 2A and 2E). The baseline for each neuron, which also served as the threshold for identifying "responding" ChIs, was determined by the mean action potential probability for each 100-ms window 2 s prior to the stimulus, plus 2 standard deviations. We did not observe a pause following the bursting activity in ChIs, as has been previously reported (Ding et al., 2010), likely due to a shorter stimulation protocol. Conversely, cortical stimulation at the same frequency and intensity did not increase the overall firing of ChIs above baseline (baseline probability: 0.22 ± 0.02; stimulus probability: 0.28 ± 0.06; n = 29, $p > 0.05$, Wilcoxon matched pair signed rank) (Figures 2B–2F). This confirms that thalamic inputs more strongly drive ChI firing than cortical inputs.

We found, however, that while stimulation of cortical inputs did not alter the average firing of ChIs, a subpopulation of ChIs did show a robust increase in firing (9/29 ChIs recorded; average cortical responder action potential (AP) probability 0.67 ± 0.1). This was reflected in the greater overall coefficient of variation (CV) for the action potential probability following cortical stimulation across all ChIs recorded (thalamus: 0.25, n = 13; cortex: 1.16, n = 29). Cortically evoked EPSPs also had a greater CV in their amplitudes (thalamus: 0.66; cortex: 0.76, n = 10 cells each) and had a shorter latency to spike relative to thalamic stimulation (cortical responders: 20.2 ± 6 ms, n = 10; thalamus: 44.74 ± 4 ms, n = 11; $p < 0.01$, Mann-Whitney) (Figure 2G).

Because cortical inputs consistently depress, we hypothesized that there is preferential connectivity to a subpopulation of ChIs, such that the amplitude of cortically evoked EPSPs may be larger in responding ChIs than in non-responders. To examine differences between ChI responders and non-responders to cortical input, we recorded a ChI in cell-attached mode and stimulated cortical inputs to determine whether the recorded cell responded to the stimulus (Figure 3A). To more clearly separate differences that might underlie this spectrum of ChI activity, we segregated neurons that responded strongly to cortical stimulation. We classified ChIs with a stimulus AP probability above 0.75 as "responders" and non-responsive ChIs with a stimulus AP probability below 0.25 as "non-responders" and tested them as such. We found that in strongly responding ChIs, EPSPs measured by re-patching the same neuron in the current clamp were significantly larger in amplitude than in ChIs that did not respond (responder: 2.6 ± 0.4 mV, n = 6; non-responder: 0.57 ± 0.2 mV, n = 6; $p < 0.01$, Mann-Whitney) (Figures 3A–3C). Further, strong responders displayed a greater area under the curve for cortically evoked EPSPs relative to non-responders (responders: 0.17 ± 0.02 mV × s; non-responders: 0.03 ± 0.009 mV × s; n = 6 for each, $p < 0.01$, Kruskal-Wallace) (Figures 3B and 3C). The area under the EPSP train accounts for the summation of individual EPSPs due to the long membrane time constant of ChIs (Kawaguchi, 1993; Wilson et al., 1990). The EPSP area was not significantly different between ChIs that responded to cortical inputs and ChIs in response to thalamic stimulation (thalamus: 0.29

± 0.1 mV × s, n = 10, $p > 0.05$ relative to cortical responders; $p < 0.05$ relative to cortical non-responders; Kruskal-Wallace) (Figures 3B and 3C).

To confirm that these differences were not simply the result of uneven expression or distribution of ChR2 across animals and experimental groups, we performed simultaneous dual recordings of two neighboring ChIs in cell-attached configurations. ChIs were selected by selectively expressing mCherry in ChIs using CaMkII-Cre;ChAT-Cre mice. The nearest of two neighboring ChIs (less than 200 μm) was recorded. Although we observed no difference in AP probability between simultaneously recorded ChIs on average (Figure S1F), the firing probability of each ChI in the pair was highly variable when driven by cortical inputs, with no significant correlation between the firing probability of any simultaneously recorded neurons (n = 4 paired recordings, Spearman's correlation, $p > 0.05$ for each) (Figures 3E and 3F). There was also no overall correlation in success rates between ChIs recorded simultaneously compared to the same ChIs when their partners were shuffled (avg. Spearman's correlation coefficient; simultaneous: −0.046 ± 0.2; non-simultaneous: 0.048 ± 0.02). This suggests that the variability in the responses of adjacent ChIs was likely due to differences in the cell-specific strength of cortical inputs rather than to differences in the extent of ChR2 expression, stimulation levels, or sites between recordings. Next, to further confirm that the variability in ChI responses was not due to differences in the extent of expression, we performed simultaneous dual recordings of ChIs (in cell-attached mode) and nearby MSNs (in voltage clamp mode). We found that while the responses of ChIs were variable, the amplitude of EPSCs in adjacent MSNs was consistent and did not correlate with the extent of firing in the neighboring ChI (cortical responder pair first EPSC amplitude: −589.4 ± 138 pA, n = 5; cortical non-responder pair first EPSC amplitude: −777.6 ± 185 pA, n = 4; $p > 0.05$, Mann-Whitney) (Figures 3G and 3H). Together, these results indicate that the variability in the expression of ChR2 across groups is unlikely to explain the variability in responses of ChIs following cortical stimulation.

While expression differences were not sufficient to explain differences in response probability, we did observe a higher AMPA/NMDA ratio in cortically responding ChIs than in non-responders (responders: 1.40 ± 0.2, n = 9; non-responders: 0.88 ± 0.1, n = 8; $p < 0.05$, Mann-Whitney) (Figures 3I and 3J). Furthermore, consistent with increased response to a given stimulus, input resistance was also higher in responders than in non-responders (responders: 89.3 ± 9 MΩ, n = 10; non-responders: 71.0 ± 8, n = 12; $p < 0.05$, Mann-Whitney) (Figure S1A). This suggests that although cortical inputs do not increase ChI firing on average, there is a subset of neurons that receive sufficient input that allows them to respond similarly to both cortical and thalamic inputs. Membrane capacitance (responders: 28.0 ± 3 pF, n = 10; non-responders: 31.0 ± 3 pF, n = 12; $p > 0.05$, Mann-Whitney), average baseline firing rate (responders: 0.96 ± 0.3 Hz, n = 10; non-responders: 0.90 ± 0.3, n = 12; $p > 0.05$, Mann-Whitney) (Figures S1B and S1C), and the extent of short-term synaptic depression (5th pulse over 1st pulse, responder voltage: 0.64 ± 4, n = 6; responder current: 0.50 ± 0.1, n = 10; non-responder voltage: 0.51 ± 0.1, n = 5; non-responder current: 0.42 ± 0.05, n = 9; $p > 0.05$, 2-way ANOVA) (Figure S1D) were similar between the two groups.

Cortical and Thalamic Excitatory Inputs Target Different Locations on ChI Dendrites

Anatomical examination of cortical and thalamic inputs onto ChIs has shown that while thalamic inputs target soma and proximal dendrites, cortical inputs are localized on distal ChI dendrites (Lapper and Bolam, 1992). To test whether the distance of these inputs from the ChI cell body might result in differences in dendritic filtering, we performed a voltage-jump experiment (Pearce, 1993; Straub et al., 2016). Because of the extensive dendritic arbor of ChIs, filtering of synaptic currents may occur, leading to slower synaptic currents at more distal dendritic sites, due to space clamp (Mainen et al., 1996; Major, 1993). ChIs were held at 0 mV, the reversal potential for AMPA receptors, such that no current would flow through open AMPA receptors. A single flash stimulus was then delivered to evoke glutamate release from either the thalamic or cortical inputs. Five milliseconds after the light pulse, the voltage was stepped to −60 mV (Figure 4A). After subtracting the capacitive transient, the resulting current is due to the driving force generated following the jump through open AMPA receptors. The rate of activation is determined by the speed by which the current can be clamped and is independent of the kinetics of AMPA receptor activation (Pearce, 1993). Because of an increased membrane time constant, distal inputs would be expected to have slower rates of activation. Using this protocol, we found that the activation time constant was significantly slower for voltage-jump currents evoked from cortical inputs (1.74 ± 0.4 ms, n = 9) than thalamic inputs (0.65 ± 0.2 ms, n = 8, $p < 0.05$, Mann-Whitney) (Figures 4B and 4C). These results suggest that cortical inputs are more distal than thalamic inputs are. As a control, to verify that the activation time constant of voltage-jump currents is slower for inputs farther from the soma, we used the same voltage protocol as above, this time using iontophoretic application of glutamate to distal and proximal dendrites. Exogenous glutamate was locally applied via an iontophoretic pipette imaged using 2-photon microscopy. The iontophoretic pipette was positioned near spines of the recorded ChIs at different distances along the same dendritic branch (Figure 4D). Repeating the voltage-jump experiment revealed that voltage-jump-evoked currents could be clamped faster when glutamate was applied to proximal dendrites (Figure 4E). The activation time constant for the more proximally evoked iontophoretic current (1.19 ± 0.3 ms) was faster than the distally evoked currents in the same cell (6.63 ± 2 ms, n = 5, $p < 0.05$, Student's paired t test) (Figures 4F and 4G). The time constants obtained when iontophoretically applying glutamate were longer than those with optogenetic stimulation of glutamate terminals, likely due to the broader activation receptors as a result of the widespread diffusion of glutamate from the iontophoretic puff of glutamate. Taken together, these data suggest that cortical and thalamic currents have differing dendritic integrations due to the location of each input.

Cortical and Thalamic Inputs Equally Drive Striatal Cholinergic Transmission

We next wanted to determine how cortical and thalamic inputs drive the release of ACh at muscarinic synapses onto MSNs. To measure the activation of muscarinic receptors, we virally overexpressed a G-protein coupled inwardly rectifying K^+ channel (GIRK2; $K_{ir}3.2$) in MSNs. Endogenous M4-muscarinic receptors couple to overexpressed GIRK2 channels, providing a rapid, direct readout of synaptic M4-receptor activation (Cai and Ford, 2018; Mamaligas and Ford, 2016). Using this approach, we previously showed that the pacemaker firing of ChIs evokes ACh release that is encoded at these synapses as a series of individual

spontaneous M4-muscarinic-inhibitory post synaptic potentials (IPSCs) in GIRK2-expressing direct pathway D1-MSNs (Mamaligas and Ford, 2016). The expression of GIRK2 does not affect MSN excitability or input resistance (Marcott et al., 2014), and expression is largely restricted from ChIs (Mamaligas and Ford, 2016).

While M1 receptors are expressed in both D1-MSNs and D2-MSNs, M4 receptors are expressed predominantly in D1-MSNs (Bernard et al., 1992; Yan et al., 2001). Scopolamine-sensitive muscarinic-IPSCs are observed in all D1-MSNs following GIRK2 expression (Mamaligas and Ford, 2016; Marcott et al., 2018). To further confirm that GIRK2$^+$ D2-MSNs do not exhibit muscarinic-IPSCs, we first selectively expressed GIRK2 in D2-MSNs by injecting AAV9.DiO.hSyn.tdTomato.T2A.GIRK2 into A2A-cre mice. We found, using this reporter line, that no D2-MSNs exhibited scopolamine-sensitive muscarinic-IPSCs (0/8 MSNs) (Figure S2). As GIRK channels preferentially couple to $G\alpha_{i/o}$-coupled G-protein coupled receptors (GPCRs) (Lüscher and Slesinger, 2010), scopolamine-sensitive muscarinic-IPSCs in D1-MSNs likely result from the activation of muscarinic M4 receptors. We therefore identified putative D1-MSNs by the presence of muscarinic M4-IPSCs.

An AAV encoding GIRK2 and a soluble tdTomato fluorophore driven by the synapsin promoter (AAV9.hSyn.tdTomato.GIRK2) was injected into the striatum, and AAV.DIO.ChR2.eYFP was injected into either the motor cortex or the parafascicular thalamus of CaMKII-cre mice. Whole-cell voltage clamp recordings were made from GIRK2$^+$ MSNs in the dorsolateral striatum (V_h = −60 mV). As cortical and thalamic inputs directly synapse onto MSNs (Ding et al., 2010; Parker et al., 2016), photoactivation (5 stimuli at 50 Hz) of both terminals evoked inward AMPA EPSCs in MSNs (Figures 5A and 5B). In putative D1-MSNs expressing GIRK2, EPSCs were followed by a slower outward muscarinic receptor-mediated M4-IPSC (Figures 5A–5C). Because of the slower kinetics of these metabotropic M4-IPSCs relative to ligand-gated ion channel currents (Mamaligas and Ford, 2016), it was possible to separately resolve the direct-input AMPA EPSCs from the disynaptic M4-IPSCs resulting from ACh release from ChIs. While we observed EPSCs in all MSNs, only ~50% of MSNs (putative D1-MSNs) exhibited the subsequent slower M4-IPSC. Evoked M4-IPSCs were only observed in MSNs that also exhibited spontaneous M4-IPSCs.

The probability of evoking an M4-IPSC in MSNs was similar when evoked by cortical and thalamic stimulation (IPSC probability – thalamus: 0.99 ± 0.005, n = 27; cortex: 0.98 ± 0.01, n = 25; $p > 0.05$, Mann-Whitney) (Figure 5D), as was the amplitude (thalamus: 189 ± 27 pA, n = 27; cortex: 186 ± 31 pA, n = 25; $p > 0.05$, Mann-Whitney) (Figure 5C). Although we saw similar amplitudes overall, viral expression of GIRK2 in the striatum is highly variable, limiting direct amplitude comparisons between cells. Bath application of 2,3-dihydroxy-6-nitro-7-sulfamoyl-benzo[f]quinoxaline (NBQX; 10 μM) and AP5 (50 μM) to block AMPA and NMDA receptors, respectively, completely eliminated both glutamatergic EPSCs and disynaptic-evoked muscarinic-IPSCs in all recordings (thalamus: 0.3% ± 0.5% remaining, n = 6; cortex: 0.2% ± 1% remaining, n = 11). Thus, unlike the difference in the extent of action potential generation in ChIs, both cortical and thalamic inputs equally evoked the release of ACh at muscarinic synapses on MSNs. We observed that both cortical and thalamic burst stimulations evoked an increase in M4-IPSC amplitudes over a single

stimulus (thalamus burst: 250.9 ± 34 pA; thalamus single: 43.8 ± 10 pA, n = 12, $p < 0.001$; cortex burst: 129.2 ± 28 pA, cortex single: 35.7 ± 7 pA, n = 11, $p < 0.01$, Wilcoxon matched pair signed rank; cortex single v thalamus single: $p > 0.05$, Mann-Whitney). To confirm the difference between action potential generation and ACh release, we also recorded from ChIs (in the current clamp) followed by adjacent GIRK2$^+$ MSNs (in voltage clamp) (Figure 5E). We found that while the firing of ChIs still varied between cortical and thalamic stimulations (cortically evoked ChI firing probability: 0.34 ± 0.1; thalamically evoked ChI firing probability: 0.73 ± 0.06), M4-IPSCs in adjacent MSNs were reliably evoked in all cases (cortically evoked M4-IPSC probability: 0.96 ± 0.03, n = 9; thalamically evoked M4-IPSC probability: 1.0, n = 8; $p > 0.05$) (Figures 5E and 5F). As the release of ACh underlying M4-IPSCs is action-potential dependent (Mamaligas and Ford, 2016), this suggests that the subpopulation of ChIs that do respond to cortical stimulation drive cortically evoked M4-IPSCs broadly onto MSNs.

ChIs converge onto D1-MSNs at independent muscarinic synapses, with several ChIs synapsing onto one MSN (Mamaligas and Ford, 2016). MSNs are capable of integrating those convergent responses in an additive manner (Mamaligas and Ford, 2016). To confirm this, we performed minimal electrical stimulation of two nearby ChIs. While recording M4-IPSCs in an adjacent GIRK2$^+$ MSN, we found that stimulation of either ChI could evoke an M4-IPSC and that the arithmetic sum of the two amplitudes was identical to the amplitude of the evoked M4-IPSC when both ChIs were stimulated simultaneously (Figures 5G and 5H). Together, the results suggest that while only a minority of ChIs fire action potentials in response to cortical input, convergence of multiple ChIs onto a given MSN compensates for this, allowing for reliable muscarinic receptor activation in MSNs even though cortical stimulation causes no increase in the overall average firing rate of ChIs. As a control, in order to confirm that this minimal electrical stimulation activates only one ChI, a monopolar stimulating electrode was placed within ~10 μm of the soma of a ChI, and a brief electrical stimulation (1 ms, 9–15 μA) was used to trigger an action potential. This minimal stimulation was sufficient to reliably trigger an action potential in the stimulated ChI but failed to evoke an action potential in an adjacent ChI (AP probability of adjacent stimulated ChI: 0.94 ± 0.06; AP probability of adjacent ChI: 0 ± 0; n = 6, $p < 0.05$, Wilcoxon matched pair signed rank).

Role of AMPA and NMDA Receptors at Cortical and Thalamic ChI Synapses

Previous work has found that dopamine release, driven by thalamic inputs to ChIs, relies on both AMPA and NMDA receptors, while cortical inputs do so primarily via AMPA receptors (Kosillo et al., 2016). To examine the contribution of different glutamate receptors on ChIs that are required to drive ACh release at muscarinic synapses, we bath applied either NBQX (10 μM) to block AMPA receptors or AP5 (50 μM) to block NMDA receptors. Following thalamic stimulation, evoked muscarinic M4-IPSCs were partially blocked in the presence of NBQX (67.9% ± 8% remaining; n = 7) (Figures 6A and 6C) but were completely eliminated in the presence of AP5 (0.42% ± 1% remaining; n = 5, $p < 0.01$, Mann-Whitney) (Figures 6B and 6C). Although the amplitude of thalamically evoked M4-IPSCs was reduced in NBQX, there was no change in the probability of evoking an IPSC (control: 1 ± 0; NBQX: 0.92 ± 0.08; n = 7, $p > 0.05$, Wilcoxon matched pair signed rank) (Figure 6E). While NBQX

was sufficient to strongly inhibit EPSPs recorded in ChIs (last pulse: 19.4% ± 6% of control amplitude; n = 5) (Figures S3A and S3B), ChI firing probability only decreased slightly (38.8% ± 9%; n = 6) (Figures S3C–S3E). Conversely, while AP5 only has a modest effect on thalamic-evoked EPSP amplitudes in ChIs (last pulse: 63.4% ± 8% of control amplitude; n = 5) (Figures S3A and S3B), it has a strong effect on ChI firing probability (14.6% ± 4% of control probability; n = 6) (Figures S3C–S3E). Thus, unlike the release of dopamine driven by ACh from ChIs (Kosillo et al., 2016), we found that the release of Ach, which evokes M4-IPSCs driven by thalamic inputs, predominantly relies upon NMDA receptors.

Following multiple excitatory stimuli, AMPA-receptor-mediated depolarization of the post-synaptic cell is often sufficient to relieve NMDA receptor Mg^{2+} block, leading to increased activity during later pulses in the stimulus (Herron et al., 1986). Although we saw no differences in AMPA/NMDA ratios following a single stimulus between cortical and thalamic inputs (Figure 1E), multiple stimuli may depolarize ChI dendrites sufficiently to unblock NMDA receptors. Because thalamic inputs facilitate (Figure 1F), these inputs might be more likely to depolarize and unblock ChI NMDA receptors. To test whether AMPA-receptor-mediated depolarization of ChI dendrites primarily functions to relieve the Mg^{2+} block of NMDA receptors, we repeated the same experiments in the presence of a Mg^{2+}-free solution. In the absence of Mg^{2+}, NBQX had no effect on M4-IPSCs (103% ± 3% of baseline amplitude; IPSC probability = 1.0; n = 6) (Figures 6F and 6H), while AP5 strongly blocked M4-IPSCs (14% ± 6% of baseline; n = 6) (Figures 6G and 6H). This suggests that the role of AMPA receptors at thalamic synapses may be to provide sufficient depolarization to unblock NMDA receptors, which ultimately drives ChI firing and ACh release.

In contrast to thalamic inputs, muscarinic M4-IPSCs evoked by optogenetic stimulation of cortical inputs were partially inhibited by both NBQX (10 μM; 30.2% ± 7% remaining; n = 5) (Figures 7A and 7C) and AP5 (50 μM; 54.2% ± 7% remaining; n = 8, $p < 0.05$ relative to NBQX, Mann-Whitney) (Figures 7B and 7C). The inhibition of AMPA receptors had a stronger effect on the amplitude of M4-IPSCs than did the inhibition of NMDA receptors (Figure 7C), but neither antagonist decreased the probability of evoking M4-IPSCs (NBQX: 0.90 ± 0.05, n = 5; AP5:1 ± 0, n = 7; $p > 0.05$ for both, Wilcoxon matched pair signed rank) (Figure 7E). Recordings in ChIs also displayed a similar inhibition for both EPSP amplitude (NBQX: 25.4% ± 9% of first pulse amplitude; AP5: 77.0% ± 6% of first pulse amplitude; n = 5 for each) (Figures S4A and S4B) and firing (NBQX: 25.9% ± 12% of control firing probability; AP5: 44.4% ± 20% of control firing probability; n = 4 for each) (Figures S4C–S4E) for both antagonists.

Because of the high release probability (P_r) of cortical inputs (Figures 1 and 3), ChIs responding to cortical stimulation likely do so on the first pulse. AMPA receptors may have a stronger effect during the first pulse because of the Mg^{2+} block on NMDA receptors. As such, in Mg^{2+}-free solutions, we found that NBQX only slightly inhibited M4-IPSCs (89.0% ± 7% of baseline remaining; n = 6), whereas AP5 had a much stronger effect on M4-IPSCs (24.6% ± 14% of baseline remaining; n = 6, $p < 0.01$ relative to NBQX, Mann-Whitney) (Figures 7F–7H), thus reversing the previous pattern of inhibition. These results confirm differences in receptor activity driving ChI activity following excitatory stimuli from the cortex and thalamus.

DISCUSSION

Stimulation of cortical and thalamic inputs to the striatum is known to drive different firing patterns in ChIs, both *in vivo* and in *ex vivo* slices (Ding et al., 2010; Doig et al., 2014). This work, along with other studies, has suggested that thalamic inputs are the primary drivers of ChI bursting activity in the striatum (Ding et al., 2010; Doig et al., 2014; Kosillo et al., 2016; Matsumoto et al., 2001). However, it has been unclear how these firing patterns are integrated to drive ACh release and cholinergic transmission in the striatum. ChIs make monosynaptic connections with MSNs and, unlike most GPCR synapses, single action potentials from ChIs release ACh sufficient to drive M4-muscarinic receptor-mediated synaptic events in MSNs. (Mamaligas and Ford, 2016). As such, M4 receptors are capable of encoding physiological firing patterns of convergent ChIs at independent synapses (Mamaligas and Ford, 2016). Using this system to examine the integration of ACh release at muscarinic synapses in response to excitatory stimulation, we found an apparent disconnect between ChI firing and ACh release at synaptic sites on MSNs. Similar to previous reports (Ding et al., 2010), thalamostriatal inputs onto ChIs strongly facilitate, leading to a high probability of ChI firing and subsequent ACh release. Conversely, corticostriatal inputs onto these cells depress, and the initial evoked EPSP is insufficient to drive an overall increase in ChI firing. However, despite the lack of increase in cortically evoked ChI firing probability for the averaged data, cortical inputs drive large EPSPs and strong subsequent activity in a subset of ChIs. This, together with differences in the relative proportion of AMPA versus NMDA receptors and input resistance, increases the overall excitability of this subpopulation of ChIs. It is likely that these cortically responding ChIs are not a new class of ChIs, but rather that they fall at one end of a spectrum of synaptic properties including afferent connectivity, input resistance, and post-synaptic integration. The net result is that cortical inputs effectively drive ACh release onto MSNs due to divergence of the responding ChIs onto multiple MSNs.

In contrast to the variability of ChI firing in response to cortical stimulation, we found that the release of ACh onto MSNs at muscarinic synapses across the striatum was highly consistent. Multiple ChIs make independent synaptic inputs onto direct pathway MSNs, and the amplitude of spontaneous muscarinic M4-IPSCs has been found to vary depending on the extent of connectivity of a presynaptic ChI to a given MSN (Mamaligas and Ford, 2016). Thus, differences between the weak overall effect on ChI firing versus the strong subsequent release of ACh likely result from the convergence of tiled ChIs with overlapping axonal fields that widely innervate multiple MSNs. ChIs have long, highly branched axons (Bolam et al., 1984; Contant et al., 1996; Descarries and Mechawar, 2000), which allow ChI to make muscarinic synapses onto D1-MSNs over a distance of at least 200 μm (Mamaligas and Ford, 2016). As ChIs in the dorsal striatum are separated from each other on average by 40–70 μm (Matamales et al., 2016), they have large overlapping axonal areas that converge onto a given MSN. As a result, when cortical inputs effectively drive ChI activity, even in a small number of interneurons, the release of ACh from those cells drives muscarinic synaptic events across multiple MSNs. As a result, we saw similar M4-IPSCs following both stimuli.

Role of Facilitation and Depression of Input-Specific ChI Activity

As the range of EPSP amplitudes evoked from both excitatory inputs were similar, differences in ChI action potential generation likely result from differences in synaptic facilitation of each input (Aceves Buendia et al., 2019; Ding et al., 2010; Kosillo et al., 2016). Because thalamic inputs onto ChIs facilitate, evoking more depolarization, the relative synaptic strength of ChIs connected to a given MSN is less important for thalamostriatal inputs. In contrast, cortically evoked EPSPs that begin below the threshold would never depolarize the ChI sufficiently to reach the threshold. Thus, targeted innervation seems to be necessary for the ChI response to cortical excitation. Our results also suggest that AMPA and NMDA receptors play different roles at cortical and thalamic synapses. At thalamic synapses, NMDA receptors provide the majority of the depolarization necessary to drive ChI firing. While AMPA receptors also contribute to thalamic-evoked ChI activity, they seem to play a lesser role; instead, we found that AMPA receptors primarily serve to sufficiently depolarize ChI dendrites, thus unblocking Mg^{2+} from NMDA receptors during facilitating bursts of thalamic stimuli. The facilitation that occurs at thalamic synapses is thus required to evoke this NMDA receptor unblock and drive higher ChI activity. This is consistent with previous reports that the inhibition of NMDA receptors strongly inhibits thalamically evoked EPSPs in ChIs (Kosillo et al., 2016). At cortical synapses, we found that AMPA receptors drive ChI firing more strongly than they do at thalamic synapses. However, contrary to previous studies (Kosillo et al., 2016), we found that NMDA receptor activity is also important for cortically evoked ChI firing. A possible explanation for the difference between the present results and those of Kosillo et al. (2016) may be due to the use of a relatively low concentration of GYKI52466 in the latter study, which may have been insufficient to fully occupy AMPA receptors. Because cortical inputs depress, summation of cortical EPSPs is not required to drive ChI firing. As AMPA receptors provide a large depolarizing conductance on the first stimulus, interactions between AMPA and NMDA receptors play a smaller role at cortical synapses onto ChIs.

Potential Roles of ChI Excitation *In Vivo*

Previous studies have shown that *in vivo*, neurons in the intralaminar thalamic nuclei increase their firing up to 60 Hz during attention tasks. Although thalamic neurons in this region show two different latencies to activity during these tasks, almost all of them showed burst activity during the task, with each burst lasting between 50 and 150 ms (Matsumoto et al., 2001). Pyramidal neurons in the motor cortices tend to burst up to 100 Hz during the preparation and execution of movements (Hall et al., 2014; Mollazadeh et al., 2011). These bursts can have multiple different patterns, including oscillatory activity, in different contexts and on different time scales (Churchland et al., 2012). Although *in vivo* stimulation of both the motor cortex and intralaminar thalamus is sufficient to drive ChIs to fire (Doig et al., 2014), there is no correlation between M1 pyramidal neuron firing and ChI activity (Sharott et al., 2012). In contrast, ChIs fail to display stereotyped bursting patterns when the parafascicular thalamic activity is inhibited (Matsumoto et al., 2001). Along with *ex vivo* firing data showing only modest increases in ChI activity following direct stimulation, this suggests that *in vivo* increases in ChI activity due to cortical excitation may occur through greater circuit mechanisms rather than due to direct excitation. The current study suggests, however, that while cortically evoked glutamate release in the striatum may not drive very

high levels of ChI firing, it might nonetheless be sufficient to drive widespread acetylcholine release. Further, as motor, somatosensory, and frontal association cortices all converge in the dorsolateral striatum, and other cortical regions project to the dorsomedial and ventral striatum (Hunnicutt et al., 2016), it is possible that each of these regions responding to different stimuli and behavioral patterns could be very important in the activation of ChIs in this subregion.

This study provides evidence that cortical inputs drive more robust ChI activity and ACh release than originally thought. The architecture and geometry of the striatum allows for MSNs to integrate the activity of several ChIs, causing reliable ACh release in response to both major striatal excitatory inputs. As thalamic inputs from the parafascicular nucleus degenerate in even mild cases of Parkinson's disease (Smith et al., 2009, 2014), ACh release evoked through cortical activity could be overrepresented during an attempted movement. This could result in an increase in ACh release during movement and a decrease during associative behaviors, causing an imbalance of MSN activity. Indeed, although there is no overall effect on MSNs, lesion of the parafascicular thalamus itself leads to decreased ChI activity and impaired goal-switching behaviors (Bradfield et al., 2013). Animals with a parafascicular lesion struggled to suppress previous associations, continuing to perform previously learned actions despite a devaluation of the reward (Bradfield et al., 2013). This suggests that, in a disease state, thalamic degeneration could evoke behavioral rigidity due to ACh imbalance.

The resulting over-representation of motor programs in the striatum may potentially amplify the Parkinsonian state. Previous work has shown that excitatory thalamic inputs onto direct pathway medium spiny neurons (dMSNs) exhibit selective degeneration in 6-hydroxydopamine (6-OHDA) models of dopamine depletion, while inputs to indirect pathway MSNs remain unaffected (Parker et al., 2016). The decrease in direct pathway MSN excitability resulting from thalamic degeneration skews striatal output to the indirect pathway. As ChI connectivity with indirect pathway MSNs increases following dopamine depletion, while connectivity with direct pathway MSNs decreases (Salin et al., 2009), ACh release would cause a preferential increase in indirect MSN activity through M1 receptors. If this is the case, then cholinergic signaling could amplify the differences between direct and indirect pathway activities, causing more excitation in indirect pathway MSNs and enhancing rigidity.

STAR★METHODS

LEAD CONTACT AND MATERIALS AVAILABILITY

Further information and requests for resources and reagents should be directed to and will be fulfilled by the Lead Contact, Christopher P. Ford (christopher.ford@ucdenver.edu).

EXPERIMENTAL MODEL AND SUBJECT DETAILS

Experimental Models—All experiments were approved by and performed in agreement with the guidelines of the Institutional Animal Care and Use Committee (IACUC) at University of Colorado School of Medicine. 6 - 8 week-old mice used in experiments were:

CaMKII-Cre heterozygote mice (generated from WT and homozygous B6.Cg-Tg(Camk2a-cre)T29-1Stl/J, Jackson Laboratory), A2a-cre mice (Tg(Adora2a-cre) KG139Gsat; MMRRC), ChAT-IRES-Cre mice (Chat$^{tim2(cre)Lowl}$/J, Jackson Laboratory) and wild-type C57BL/6J mice (Jackson Laboratory). Both male and female mice were used for all experiments.

Subject Details

Stereotaxic Injections: Male and female CaMKII-Cre heterozygote mice (generated from WT and homozygous B6.Cg-Tg(Camk2a-cre)T29-1Stl/J, Jackson Laboratory) were anesthetized with isoflurane and mounted in a stereotaxic frame (Kopf Instruments). Mice were injected using a nanoject iii microinjector (Drummond Scientific) between postnatal day 21 and 28 with 500 nL of AAV5.EF1a.DIO.hChR2(H134R)-EYFP.WPRE.hGH (ChR2) into one hemisphere of either the parafascicular thalamus (coordinates relative to bregma: AP −1.65, ML −0.85, DV −3.4) or the motor cortex (AP +1.1, ML −1.45, DV −1.2). For experiments requiring expression of GIRK2, 400 nL of AAV9.hSyn.tdTomato.T2A.mGIRK2-1-A22A.WPRE.bGH were also injected into the striatum (AP +1.15, ML −1.8, DV −3.3). Animals were allowed to recover for at least 3 weeks following surgery. All AAVs were from University of Pennsylvania Viral Core or Addgene. In a subset of experiments in order to confirm that D2-MSNs expressing GIRK2 do not exhibit M4-IPSCs, AAV9.DiO.hSyn.tdTomato.T2A.mGIRK2-1-A2A.WPRE.bGH (400 nL) was injected into the striatum of heterozygous A2a-cre mice (Tg(Adora2a-cre) KG139Gsat; MMRRC) (AP +1.15, ML −1.8, DV −3.3). For simultaneous ChI recording experiments, ChAT-IRES-Creand CaMKii-Cre heterozygous mice (generated from homozygous B6;129S6-Chat$^{tim2(cre)Lowl}$/J and B6.Cg-Tg(Camk2a-cre)T29-1Stl/J mice, Jackson Laboratory) were injected with ChR2 in the motor cortex and AAV5.EF1a.DIO.mCherry in the dorsal striatum.

METHOD DETAILS

Fluorescence Imaging—Following deep isoflurane anesthesia, AAV.ChR2-injected animals were transcardially perfused with phosphate buffered saline (PBS) containing 137 mM NaCl, 1.5 mM KH_2PO_4, 8 mM NaH_2PO_4, and 2.7 mM KCl (pH = 7.4), followed by 4% paraformaldehyde in PBS. Brains were cryoprotected overnight in 30% sucrose solution and then frozen and embedded in Neg-50 frozen section medium (Richard-Allan Scientific). Coronal slices (30 μm) were taken on a cryostat and directly mounted to the slides. Fluorescence images were then taken with a 10x objective using an Olympus BX61VS slide-scanning microscope.

Slice Preparation—Animals were transcardially perfused with ice-cold sucrose solution and then decapitated. Coronal slices containing the striatum (240 μm) were obtained in the same ice-cold sucrose cutting solution containing (in mM): 75 NaCl, 2.5 KCl, 6 $MgCl_2$, 0.1 $CaCl_2$, 2 NaH_2PO_4, 25 $NaHCO_3$, 2.5 D-glucose, 50 sucrose, and 1 kyneurenic acid, bubbled with 95% O_2 and 5% CO_2. Slices were incubated at 34°C for 1 hour in aCSF containing (in mM): 126 NaCl, 2.5 KCl, 1.2 $MgCl_2$, 2.4 $CaCl_2$, 1.2 NaH_2PO_4, 21.4 $NaHCO_3$, and 11.1 D-glucose, bubbled with 95% O_2 and 5% CO_2. Slices were then transferred to the recording chamber and perfused with aCSF (34 ± 2°C) at a rate of 2 mL/min. Solutions contained

picrotoxin (100 μM) unless otherwise noted. Striatal neurons were visualized using a BXWI51 microscope (Olympus) with IR gradient contrast optics and custom-made LEDs.

Electrophysiology—Recordings were performed using an Axopatch 200B amplifier (Molecular Devices). ChIs were identified with a large h-current when stepped to −90 mV in voltage clamp and by the size of the soma. Patch pipettes (1.5-2 MΩ) used for MSN recordings and current-clamp recordings in ChIs contained: 135 mM D-gluconic acid (K), 10 mM HEPES (K) 0.1 mM $CaCl_2$, 2 mM $MgCl_2$, 10 mM BAPTA, 10 mg/mLATP, 1 mg/mL GTP, and 15 mg/mL sodium phospho-creatine, pH = 7.4,275 mOsm. Patch pipettes used for all ChI voltage clamp recordings contained: 135 mM CsCl, 0.1 mM $CaCl_2$, 2 mM $MgCl_2$, 10 mM HEPES (K), 0.1 mM EGTA, 10 mM QX-314, 10 mg/mL ATP, 1 mg/mL GTP, and 15 mg/mL sodium phospho-creatine, pH = 7.4, 275 mOsm. All recordings were acquired with Axograph X (Axograph Scientific) at 10 kHz. MSNs were held at a voltage of −60 mV. No series resistance compensation was used, and cells were discarded if their series resistance exceeded 15 MU. All drugs were bath applied via perfusion unless otherwise noted. Glutamate was applied via iontophoresis (150 mM, 160 nA ejection, 200-400 ms; 1 pulse/2 minutes). The firing rate of ChIs was between 0.3 and 3.6 Hz, similar to the range of previous slice electrophysiology studies (Bennett and Wilson, 1999).

In a subset of experiments performed in regular aCSF, addition of the $GABA_a$ receptor antagonist picrotoxin (100 μM) had no effect on the ability of either cortical inputs (responders or non-responders) or thalamic inputs to drive ChI firing, indicating that blocking $GABA_a$ receptors does not influence the extent to which afferent optogenetic stimulation alters ChI activity or the differential responses to cortical versus thalamic stimulation (n = 4 - 6, $p > 0.05$ for all, Wilcoxon matched pair signed rank) (Figure S1E).

During voltage jump recordings, ChIs were held at −60 mV. ChIs were stepped to 0 mV for 3 s before the light stimulus. ChIs were then jumped back to −60 mV 5 ms after the light stimulus. These trials were interleaved with trials without the light stimulus, and the capacitive artifact was subtracted. During iontophoresis experiments, the delay between the stimulus and the jump from 0 mV to −60 mV was approximately 5 s.

Optogenetics—ChR2 excitation was evoked with widefield 470 nm blue light from a LED (M470L3; ThorLabs) (2 ms per pulse, ~10 mW when measured at the level of the back aperture of the objective). Input output curves were initially performed by stimulating cortical and thalamic inputs to determine the light intensity required to evoke maximal amplitude EPSCs. Similar levels of light intensity evoked maximal amplitude EPSC from each pathway. The power level was then doubled to ensure sufficient maximal stimulation of ChR2 of both pathways. This level of light stimulation was used for all experiments. No attempt was made to determine if a similar number of afferent fibers were activated for each input. However only ChIs with EPSCs > 25 pA were used. In all cases the accuracy of the target injection site was verified and animals were discarded if the injection site was off target and limited $eYFP^+$ fluorescent fibers were observed in the dorsolateral striatum. A single pulse (2 ms per pulse, ~10 mW when measured at the level of the back aperture of the objective) was used for experiments to calculate AMPA/NMDA ratios (Figures 1 and 3) and for voltage jump experiments (Figure 4). All other experiments used a train of five pulses (2

ms per pulse, 50 Hz, ~10 mW when measured at the level of the back aperture of the objective) as has been used in previous studies (Aceves Buendia et al., 2019; Ding et al., 2010; Kosillo et al., 2016).

2-Photon Imaging—Images were visualized with a BX5WI microscope (Olympus) and a home built 2-photon laser scanning microscopy system run on custom code (Toronado; Ben Strowbridge) using XY galvanometer mirrors (6215, Cambridge Technology). A Mira 900 Ti:sapphire laser with a Verdi G10 pump laser (Coherent) was tuned to 800 nm. Epifluorescence signals were measured through a 60x water immersion objective (Olympus) using a T700LPXXR dichroic mirror, ET680sp and ET620/60 filters (Chroma), and a H10721-20 photo-multiplier tube (Hamamatsu). A SR570 current preamplifier (Stanford Research Systems) converted output to voltage. The voltage was digitized using an NI PCI-6110 data acquisition board (National Instruments). Alexa 594 (20 μM) in the patch pipette allowed for visualization of ChIs. Internal solution for these experiments also contained: 135 mM CsCl, 0.1 mM $CaCl_2$, 2 mM $MgCl_2$, 10 mM HEPES (K), 0.1 mM EGTA, 10 mM QX-314, 10 mg/mL ATP, 1 mg/mL GTP, and 15 mg/mL sodium phospho-creatine, pH = 7.4, 275 mOsm. For glutamate iontophoresis, a thin-walled glass iontophoretic electrode was filled with glutamate (1 M) with sulforhodamine 101 (300 μM) and was dipped in a solution containing BSA-conjugated Alexa 594 (0.06%) for ~30 s. Glutamate was injected as an anion in 250 – 500 ms pulses. Glutamate leakage was prevented with a retention current of ~20 nA.

Materials—Picrotoxin was obtained from Abcam. QX314, NBQX, and AP5 were obtained from Tocris. BAPTA was from Invitrogen. All other chemicals were from Sigma-Aldrich.

QUANTIFICATION AND STATISTICAL ANALYSIS

Statistics and Analysis—Peristimulus time histograms, constructed around the stimulus in 100 ms time bins, were used to quantify and detect stimulus-evoked ChI excitation over time in Figure 2. A permutation test was used to compare the baseline firing frequency (in shuffled 100 ms bins) 10 s prior to the stimulus with the 100 ms stimulus window. ChIs considered responders were designated when their AP firing probability was greater than that at baseline. The baseline probability (shown as a dashed line in Figures 5, S3, and S4) was taken as the mean + 2 standard deviations of the AP probability for each 100 ms time bin for 2 s prior to the stimulus. As the average baseline AP probability was near 0.25, for experiments examining cortical responders and non-responders, strongly-responding ChIs with an AP firing probability above 0.75 were designated as “responders,” and ChIs with an AP firing probability below 0.25 were designated as “non-responders.” These criteria were chosen to most easily determine differences in synaptic properties that might lead to increased cortically-evoked ChI activity. Neurons with firing probabilities between 0.25 and 0.75 were not included. To determine AP firing probability as well as M4-IPSC probability, a minimum of 7 trials were used for each neuron recorded.

Data are shown as mean ± SEM. Statistical significance was determined using Wilcoxon matched-pair signed rank test, Mann-Whitney, 2-Way ANOVA, Student’s paired t test, or Kruskal-Wallace tests where appropriate (Prism, Graphpad).

Supplementary Material

Refer to Web version on PubMed Central for supplementary material.

ACKNOWLEDGMENTS

This work was funded by NIH grants R01-NS95809 and R01-DA35821 (C.P.F.) and F32-DA43924 (K.B.). We thank Yuan Cai and Michael Grybko for help with cell-attached experiments, Sarah Zych for help with fluorescence microscopy, and Ben Strowbridge for providing custom software for 2 photon imaging.

REFERENCES

Aceves Buendia JJ, Tiroshi L, Chiu WH, and Goldberg JA (2019). Selective remodeling of glutamatergic transmission to striatal cholinergic interneurons after dopamine depletion. Eur. J. Neurosci 49, 824–833. [PubMed: 28922504]

Aosaki T, Kimura M, and Graybiel AM (1995). Temporal and spatial characteristics of tonically active neurons of the primate's striatum. J. Neurophysiol 73, 1234–1252. [PubMed: 7608768]

Apicella P, Legallet E, and Trouche E (1997). Responses of tonically discharging neurons in the monkey striatum to primary rewards delivered during different behavioral states. Exp. Brain Res 116, 456–466. [PubMed: 9372294]

Bennett BD, and Wilson CJ (1999). Spontaneous activity of neostriatal cholinergic interneurons in vitro. J. Neurosci 19, 5586–5596. [PubMed: 10377365]

Bernard V, Normand E, and Bloch B (1992). Phenotypical characterization of the rat striatal neurons expressing muscarinic receptor genes. J. Neurosci 12, 3591–3600. [PubMed: 1527598]

Bolam JP, Wainer BH, and Smith AD (1984). Characterization of cholinergic neurons in the rat neostriatum. A combination of choline acetyltransferase immunocytochemistry, Golgi-impregnation and electron microscopy. Neuroscience 12, 711–718. [PubMed: 6382048]

Bradfield LA, Bertran-Gonzalez J, Chieng B, and Balleine BW (2013). The thalamostriatal pathway and cholinergic control of goal-directed action: interlacing new with existing learning in the striatum. Neuron 79, 153–166. [PubMed: 23770257]

Brown MTC, Tan KR, O'Connor EC, Nikonenko I, Muller D, and Liischer C (2012). Ventral tegmental area GABA projections pause accumbal cholinergic interneurons to enhance associative learning. Nature 492, 452–456. [PubMed: 23178810]

Cachope R, Mateo Y, Mathur BN, Irving J, Wang H-L, Morales M, Lovinger DM, and Cheer JF (2012). Selective activation of cholinergic interneurons enhances accumbal phasic dopamine release: setting the tone for reward processing. Cell Rep. 2, 33–41. [PubMed: 22840394]

Cai Y, and Ford CP (2018). Dopamine cells differentially regulate striatal cholinergic transmission across regions through corelease of dopamine and glutamate. Cell Rep. 25, 3148–3157.e3. [PubMed: 30540946]

Churchland MM, Cunningham JP, Kaufman MT, Foster JD, Nuyujukian P, Ryu SI, and Shenoy KV (2012). Neural population dynamics during reaching. Nature 487, 51–56. [PubMed: 22722855]

Contant C, Umbriaco D, Garcia S, Watkins KC, and Descarries L (1996). Ultrastructural characterization of the acetylcholine innervation in adult rat neostriatum. Neuroscience 71, 937–947. [PubMed: 8684624]

Dautan D, Huerta-Ocampo I, Witten IB, Deisseroth K, Bolam JP, Gerdjikov T, and Mena-Segovia J (2014). A major external source of cholinergic innervation of the striatum and nucleus accumbens originates in the brainstem. J. Neurosci 34, 4509–4518. [PubMed: 24671996]

Descarries L, and Mechawar N (2000). Ultrastructural evidence for diffuse transmission by monoamine and acetylcholine neurons of the central nervous system. Prog. Brain Res 125, 27–47. [PubMed: 11098652]

Ding J, Peterson JD, and Surmeier DJ (2008). Corticostriatal and thalamostriatal synapses have distinctive properties. J. Neurosci 28, 6483–6492. [PubMed: 18562619]

Ding JB, Guzman JN, Peterson JD, Goldberg JA, and Surmeier DJ (2010). Thalamic gating of corticostriatal signaling by cholinergic interneurons. Neuron 67, 294–307. [PubMed: 20670836]

Doig NM, Magill PJ, Apicella P, Bolam JP, and Sharott A (2014). Cortical and thalamic excitation mediate the multiphasic responses of striatal cholinergic interneurons to motivationally salient stimuli. J. Neurosci 34, 3101–3117. [PubMed: 24553950]

English DF, Ibanez-Sandoval O, Stark E, Tecuapetla F, Buzsaki G, Deisseroth K, Tepper JM, and Koos T (2011). GABAergic circuits mediate the reinforcement-related signals of striatal cholinergic interneurons. Nat. Neurosci 15, 123–130. [PubMed: 22158514]

Gerfen CR (1992). The neostriatal mosaic: multiple levels of compartmental organization. Trends Neurosci. 15, 133–139. [PubMed: 1374971]

Goldberg JA, Ding JB, and Surmeier DJ (2012). Muscarinic modulation of striatal function and circuitry. Handb. Exp. Pharmacol 208, 223–241.

Graybiel AM, Aosaki T, Flaherty AW, and Kimura M (1994). The basal ganglia and adaptive motor control. Science 265, 1826–1831. [PubMed: 8091209]

Hall TM, deCarvalho F, and Jackson A (2014).Acommon structure underlies low-frequency cortical dynamics in movement, sleep, and sedation. Neuron 83, 1185–1199. [PubMed: 25132467]

Herron CE, Lester RA, Coan EJ, and Collingridge GL (1986). Frequency-dependent involvement of NMDA receptors in the hippocampus: a novel synaptic mechanism. Nature 322, 265–268. [PubMed: 2874493]

Hersch SM, Gutekunst C-A, Rees HD, Heilman CJ, and Levey AI (1994). Distribution of m1-m4 muscarinic receptor proteins in the rat striatum: light and electron microscopic immunocytochemistry using subtype-specific antibodies. J. Neurosci 14, 3351–3363. [PubMed: 8182478]

Higley MJ, Soler-Llavina GJ, and Sabatini BL (2009). Cholinergic modulation of multivesicular release regulates striatal synaptic potency and integration. Nat. Neurosci 12, 1121–1128. [PubMed: 19668198]

Hunnicutt BJ, Long BR, Kusefoglu D, Gertz KJ, Zhong H, and Mao T (2014). A comprehensive thalamocortical projection map at the mesoscopic level. Nat. Neurosci 17, 1276–1285. [PubMed: 25086607]

Hunnicutt BJ, Jongbloets BC, Birdsong WT, Gertz KJ, Zhong H, and Mao T (2016). A comprehensive excitatory input map of the striatum reveals novel functional organization. eLife 5, e19103. [PubMed: 27892854]

Kawaguchi Y (1993). Physiological, morphological, and histochemical characterization of three classes of interneurons in rat neostriatum. J. Neurosci 13, 4908–4923. [PubMed: 7693897]

Kosillo P, Zhang Y-F, Threlfell S, and Cragg SJ (2016). Cortical Control of Striatal Dopamine Transmission via Striatal Cholinergic Interneurons. Cereb. Cortex 26, 4160–4169.

Kreitzer AC (2009). Physiology and pharmacology of striatal neurons. Annu. Rev. Neurosci 32, 127–147. [PubMed: 19400717]

Lapper SR, and Bolam JP (1992). Input from the frontal cortex and the parafascicular nucleus to cholinergic interneurons in the dorsal striatum of the rat. Neuroscience 51, 533–545. [PubMed: 1488113]

Lim SAO, Kang UJ, and McGehee DS (2014). Striatal cholinergic interneuron regulation and circuit effects. Front. Synaptic Neurosci 6, 22. [PubMed: 25374536]

Lüscher C, and Slesinger PA (2010). Emerging roles for G protein-gated inwardly rectifying potassium (GIRK) channels in health and disease. Nat. Rev. Neurosci 11, 301–315. [PubMed: 20389305]

Mainen ZF, Carnevale NT, Zador AM, Claiborne BJ, and Brown TH (1996). Electrotonic architecture of hippocampal CA1 pyramidal neurons based on three-dimensional reconstructions.J. Neurophysiol 76, 1904–1923. [PubMed: 8890303]

Major G (1993). Solutions for transients in arbitrarily branching cables: III. Voltage clamp problems. Biophys. J 65, 469–491. [PubMed: 8369450]

Mamaligas AA, and Ford CP (2016). Spontaneous Synaptic Activation of Muscarinic Receptors by Striatal Cholinergic Neuron Firing. Neuron 91, 574–586. [PubMed: 27373830]

Mamaligas AA, Cai Y, and Ford CP (2016). Nicotinic and opioid receptor regulation of striatal dopamine D2-receptor mediated transmission. Sci. Rep 6, 37834. [PubMed: 27886263]

Marcott PF, Mamaligas AA, and Ford CP (2014). Phasic dopamine release drives rapid activation of striatal D2-receptors. Neuron 84, 164–176. [PubMed: 25242218]

Marcott PF, Gong S, Donthamsetti P, Grinnell SG, Nelson MN, Newman AH, Birnbaumer L, Martemyanov KA, Javitch JA, and Ford CP (2018). Regional Heterogeneity of D2-Receptor Signaling in the Dorsal Striatum and Nucleus Accumbens. Neuron 98, 575–587.e4. [PubMed: 29656874]

Matamales M, Gotz J, and Bertran-Gonzalez J (2016). Quantitative Imaging of Cholinergic Interneurons Reveals a Distinctive Spatial Organization and a Functional Gradient across the Mouse Striatum. PLoS ONE 11, e0157682. [PubMed: 27314496]

Matsumoto N, Minamimoto T, Graybiel AM, and Kimura M (2001). Neurons in the thalamic CM-Pf complex supply striatal neurons with information about behaviorally significant sensory events. J. Neurophysiol 85, 960–976. [PubMed: 11160526]

Maurice N, Liberge M, Jaouen F, Ztaou S, Hanini M, Camon J, Deisseroth K, Amalric M, Kerkerian-Le Goff L, and Beurrier C (2015). Striatal Cholinergic Interneurons Control Motor Behavior and Basal Ganglia Function in Experimental Parkinsonism. Cell Rep 13, 657–666. [PubMed: 26489458]

Mollazadeh M, Aggarwal V, Davidson AG, Law AJ, Thakor NV, and Schieber MH (2011). Spatiotemporal variation of multiple neurophysiological signals in the primary motor cortex during dexterous reach-to-grasp movements. J. Neurosci 31, 15531–15543. [PubMed: 22031899]

Morris G, Arkadir D, Nevet A, Vaadia E, and Bergman H (2004). Coincident but distinct messages of midbrain dopamine and striatal tonically active neurons. Neuron 43, 133–143. [PubMed: 15233923]

Nelson AB, Hammack N, Yang CF, Shah NM, Seal RP, and Kreitzer AC (2014). Striatal cholinergic interneurons Drive GABA release from dopamine terminals. Neuron 82, 63–70. [PubMed: 24613418]

Parker PRL, Lalive AL, and Kreitzer AC (2016). Pathway-Specific Remodeling of Thalamostriatal Synapses in Parkinsonian Mice. Neuron 89, 734–740. [PubMed: 26833136]

Pearce RA (1993). Physiological evidence for two distinct GABAA responses in rat hippocampus. Neuron 10, 189–200. [PubMed: 8382497]

Perez-Rosello T, Figueroa A, Salgado H, Vilchis C, Tecuapetla F, Guzman JN, Galarraga E, and Bargas J (2005). Cholinergic control of firing pattern and neurotransmission in rat neostriatal projection neurons: role of CaV2.1 and CaV2.2 Ca2+ channels. J. Neurophysiol 93, 2507–2519. [PubMed: 15615835]

Reynolds JN, and Wickens JR (2004). The corticostrial input to giant aspiny interneurons in the rat: a candidate pathway for synchronising the response to reward-related cues. Brain Res. 1011, 115–128. [PubMed: 15140651]

Salin P, López IP, Kachidian P, Barroso-Chinea P, Rico AJ, Gómez-Bautista V, Coulon P, Kerkerian-Le Goff L, and Lanciego JL (2009). Changes to interneuron-driven striatal microcircuits in a rat model of Parkinson's disease. Neurobiol. Dis 34, 545–552. [PubMed: 19341798]

Sharott A, Doig NM, Mallet N, and Magill PJ (2012). Relationships between the firing of identified striatal interneurons and spontaneous and driven cortical activities in vivo. J. Neurosci 32, 13221–13236. [PubMed: 22993438]

Smith Y, Raju D, Nanda B, Pare J-F, Galvan A, and Wichmann T (2009). The thalamostriatal systems: anatomical and functional organization in normal and parkinsonian states. Brain Res. Bull 78, 60–68. [PubMed: 18805468]

Smith Y, Galvan A, Ellender TJ, Doig N, Villalba RM, Huerta-Ocampo I, Wichmann T, and Bolam JP (2014). The thalamostriatal system in normal and diseased states. Front. Syst. Neurosci 8, 5. [PubMed: 24523677]

Stalnaker TA, Berg B, Aujla N, and Schoenbaum G (2016). Cholinergic Interneurons Use Orbitofrontal Input to Track Beliefs about Current State. J. Neurosci 36, 6242–6257. [PubMed: 27277802]

Straub C, Saulnier JL, Bègue A, Feng DD, Huang KW, and Sabatini BL (2016). Principles of Synaptic Organization of GABAergic Interneurons in the Striatum. Neuron 92, 84–92. [PubMed: 27710792]

Threlfell S, Lalic T, Platt NJ, Jennings KA, Deisseroth K, and Cragg SJ (2012). Striatal dopamine release is triggered by synchronized activity in cholinergic interneurons. Neuron 75, 58–64. [PubMed: 22794260]

Wilson CJ, Chang HT, and Kitai ST (1990). Firing patterns and synaptic potentials of identified giant aspiny interneurons in the rat neostriatum. J. Neurosci 10, 508–519. [PubMed: 2303856]

Yamamoto K, Ebihara K, Koshikawa N, and Kobayashi M (2013). Reciprocal regulation of inhibitory synaptic transmission by nicotinic and muscarinic receptors in rat nucleus accumbens shell. J. Physiol 591, 5745–5763. [PubMed: 24018951]

Yan Z, Flores-Hernandez J, and Surmeier DJ (2001). Coordinated expression of muscarinic receptor messenger RNAs in striatal medium spiny neurons. Neuroscience 103, 1017–1024. [PubMed: 11301208]

Zhang YF, Reynolds JNJ, and Cragg SJ (2018). Pauses in Cholinergic Interneuron Activity Are Driven by Excitatory Input and Delayed Rectification, with Dopamine Modulation. Neuron 98, 918–925.e3. [PubMed: 29754751]

Highlights

- Thalamic inputs drive firing in cholinergic cells and increase acetylcholine release
- While cortical inputs do not affect mean cholinergic activity, some cells do respond
- Cholinergic cells showing strong cortical responses have higher cortical connectivity
- Thalamic and cortical inputs drive equal acetylcholine release at muscarinic synapses

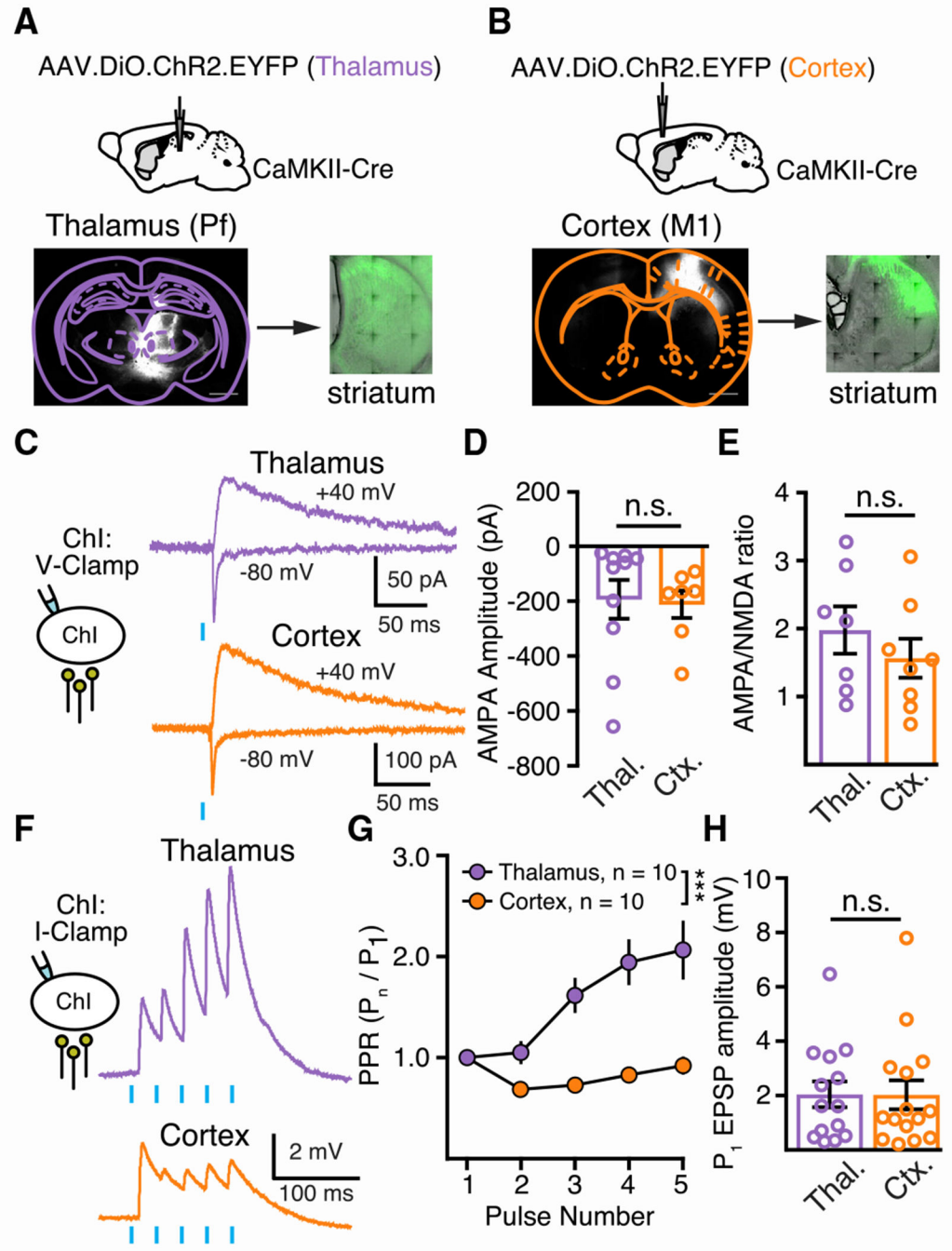

Figure 1. Optogenetic Activation of Excitatory Thalamic and Cortical Inputs Evokes Differential Short-Term Plasticity in ChIs

(A and B) Injection schematic and representative fluorescent image of AAV-induced expression of floxed ChR2 and eYFP in the parafascicular nucleus of the thalamus (A) and motor cortex (B) in CaMKii-Cre mice and their representative projection targets. Scale bars represent 500 μm.

(C) Example traces of AMPA (V_h = −80 mV) and NMDA (V_h = +40 mV) receptor-mediated currents, recorded in ChIs, evoked optogenetically (single pulse, 2 ms, 470 nm) via thalamic (purple) and cortical (orange) inputs.

(D) No differences in ChI AMPA EPSC amplitudes were found between thalamic and cortical inputs (thalamus: n = 10; cortex: n = 7; $p > 0.05$, Mann-Whitney). Error bars indicate ± SEM.

(E) No difference in AMPA/NMDA ratios between thalamic and cortical inputs (thalamus: n = 7; cortex: n = 8; $p > 0.05$, Mann-Whitney). Error bars indicate ± SEM.

(F) Representative traces of current clamp recordings in ChIs illustrating the facilitation of thalamic inputs (purple) and depression of cortical inputs (orange) in response to a burst stimulus (5 pulses, 50 Hz).

(G) Summary data displaying EPSP facilitation in thalamic inputs and EPSP depression in cortical inputs (n = 10 for each group; $p < 0.001$, 2-way ANOVA). Error bars indicate ± SEM.

(H) No difference in the amplitude of the first EPSP in the burst stimulus (thalamus: n = 14; cortex: n = 15; $p > 0.05$, Mann-Whitney). Error bars indicate ± SEM.

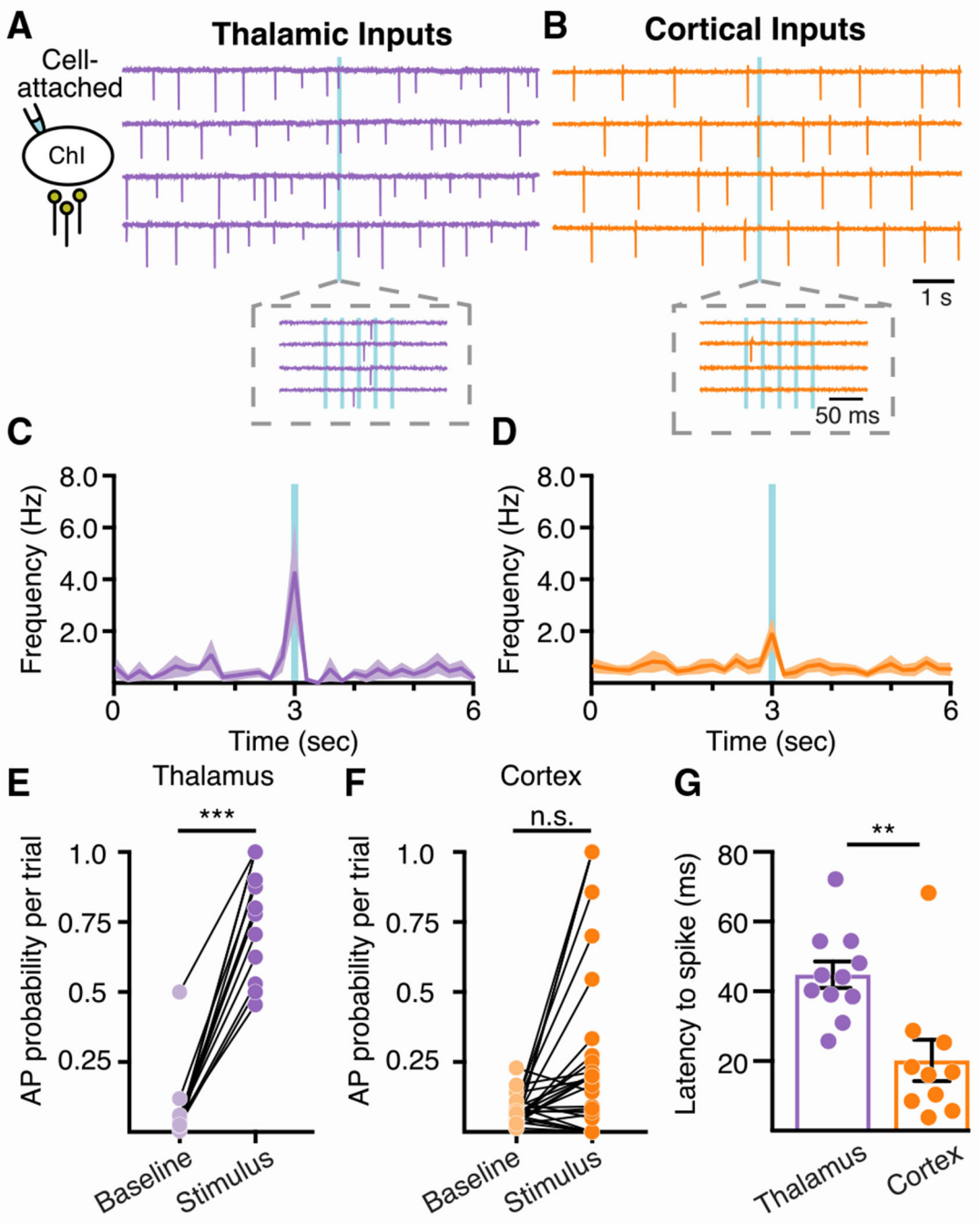

Figure 2. Differential Responses of ChIs to Thalamic and Cortical Stimuli

(A) Representative cell-attached recording of a ChI illustrating high average firing response rate due to thalamic burst stimulus (5 pulses, 50 Hz, 470 nm). Inset: zoom of stimulation period.

(B) Representative cell-attached recording of a ChI illustrating low average firing response due to cortical burst stimulus (5 pulses, 50 Hz, 470 nm). Inset: zoom of stimulation period.

(C and D) Peristimulus time histograms of ChI firing frequency during stimulation of either thalamic (C) or cortical (D) input. Error indicates ± SEM.

(E) Summary comparison of baseline ChI action potential probability during each trial with the probability during the 100-ms thalamic stimulus period ($n = 13$; $p < 0.001$, Wilcoxon matched pair signed rank), indicating a strong increase in ChI activity following thalamic stimulation, whereas cortical inputs selectively activate a subset of ChIs during the same stimulus (thalamus: $n = 13$; cortex: $n = 29$; $p < 0.001$, Mann-Whitney).
(F) Summary comparison of baseline ChI action potential probability during each trial with the probability during the 100-ms cortical stimulus period ($n = 29$; $p > 0.05$, Wilcoxon matched pair signed rank). Although ChIs are overall unresponsive to cortical excitation, some neurons increase their activity due to the stimulus.
(G) Distribution of spike latencies for responding ChIs following thalamic or cortical stimulation (thalamus: $n = 11$; cortex: $n = 10$; $p < 0.01$, Mann-Whitney). $^{**}p < 0.01$, $^{***}p < 0.001$. Error bars indicate ± SEM.

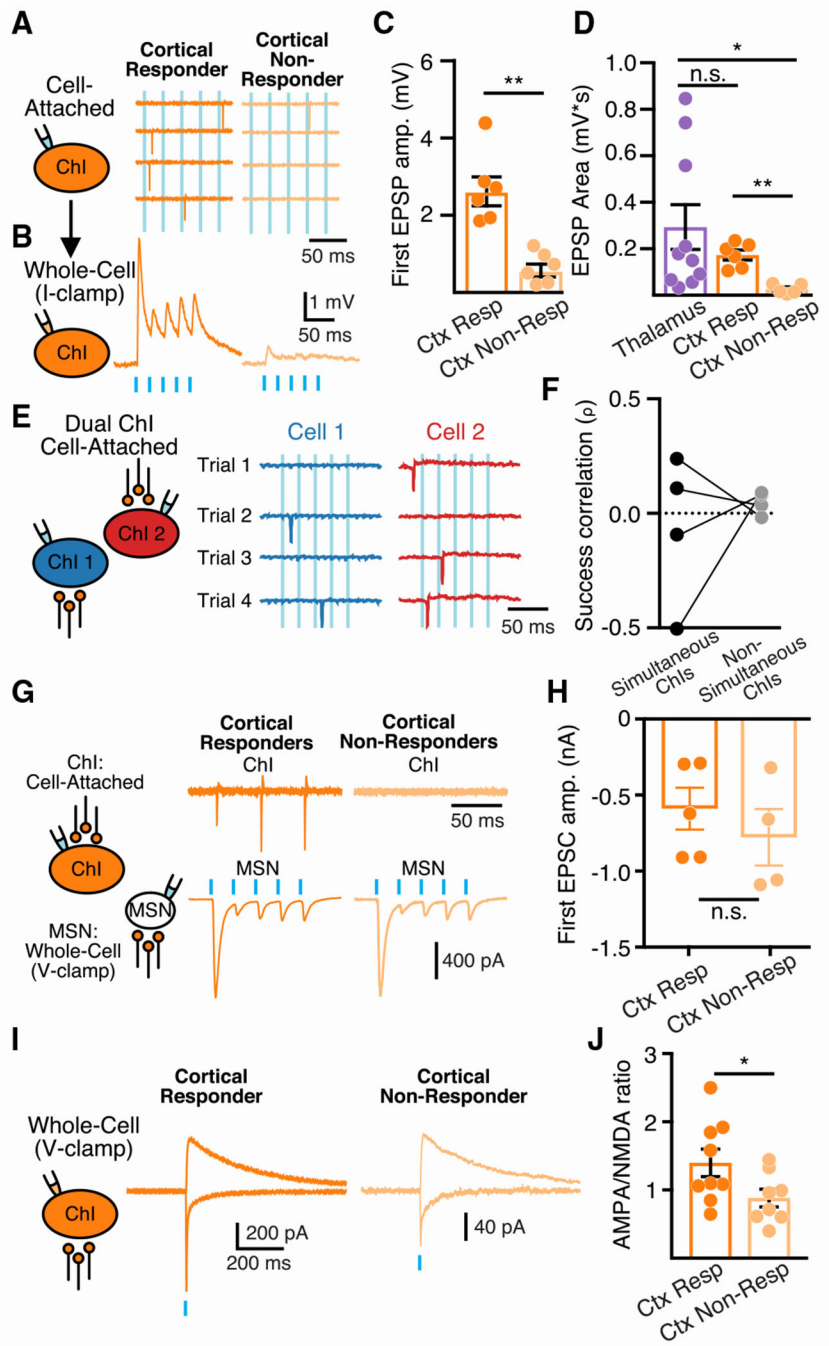

Figure 3. ChIs Show Differences in the Connectivity to Cortical Inputs

(A) Representative cell-attached recordings of ChIs illustrating responding (orange) and non-responding (peach) neurons to the same cortical stimulus.

(B) Representative EPSPs from current clamp recordings corresponding to the ChIs recorded in (D), as well as thalamically evoked EPSPs (purple).

(C) Distribution of EPSP amplitudes from ChIs that respond and do not respond to cortical stimuli (n = 6 for both groups; $p < 0.01$, Mann-Whitney). Error bars indicate ± SEM.

(D) Distribution of EPSP area for thalamically evoked EPSPs, cortical responder EPSPs, and cortical non-responder EPSPs (thalamus: n = 10; cortical responders: n = 6; cortical non-responders: n = 6; Kruskal-Wallace). *p < 0.05, **p < 0.01. Error bars indicate ± SEM.
(E) Representative simultaneous cell-attached recordings of ChIs (within 200 ¼m) illustrating that differential ChI response is not the result of ChR2 expression issues.
(F) Correlation of AP success rates within simultaneous ChI recordings, as shown in (E), compared to non-simultaneous ChI recordings (n = 4 paired recordings; Spearman's correlation).
(G) Representative dual recordings of cortically responding and non-responding ChIs (cell-attached) and MSNs (voltage clamp, V_h = −60 mV) within 100 μm. Top: individual cell-attached recording traces in ChIs; bottom: averaged EPSCs in MSNs.
(H) Distribution of EPSC amplitudes in MSNs showing similar EPSC amplitudes for striatal areas with cortically responding versus non-responding ChIs (n = 5 for both groups; Mann-Whitney). Error bars indicate ± SEM.
(I) Example traces of AMPA (V_h = −80 mV) and NMDA (V_h = +40 mV) receptor mediated currents, recorded in cortically responding and non-responding ChIs, evoked via cortical stimulation.
(J) Cortical responders (n = 9) showed a larger AMPA/NMDA ratio than did cortical non-responders (n = 8; p < 0.05, Mann-Whitney). *p < 0.05. Error bars indicate ± SEM.

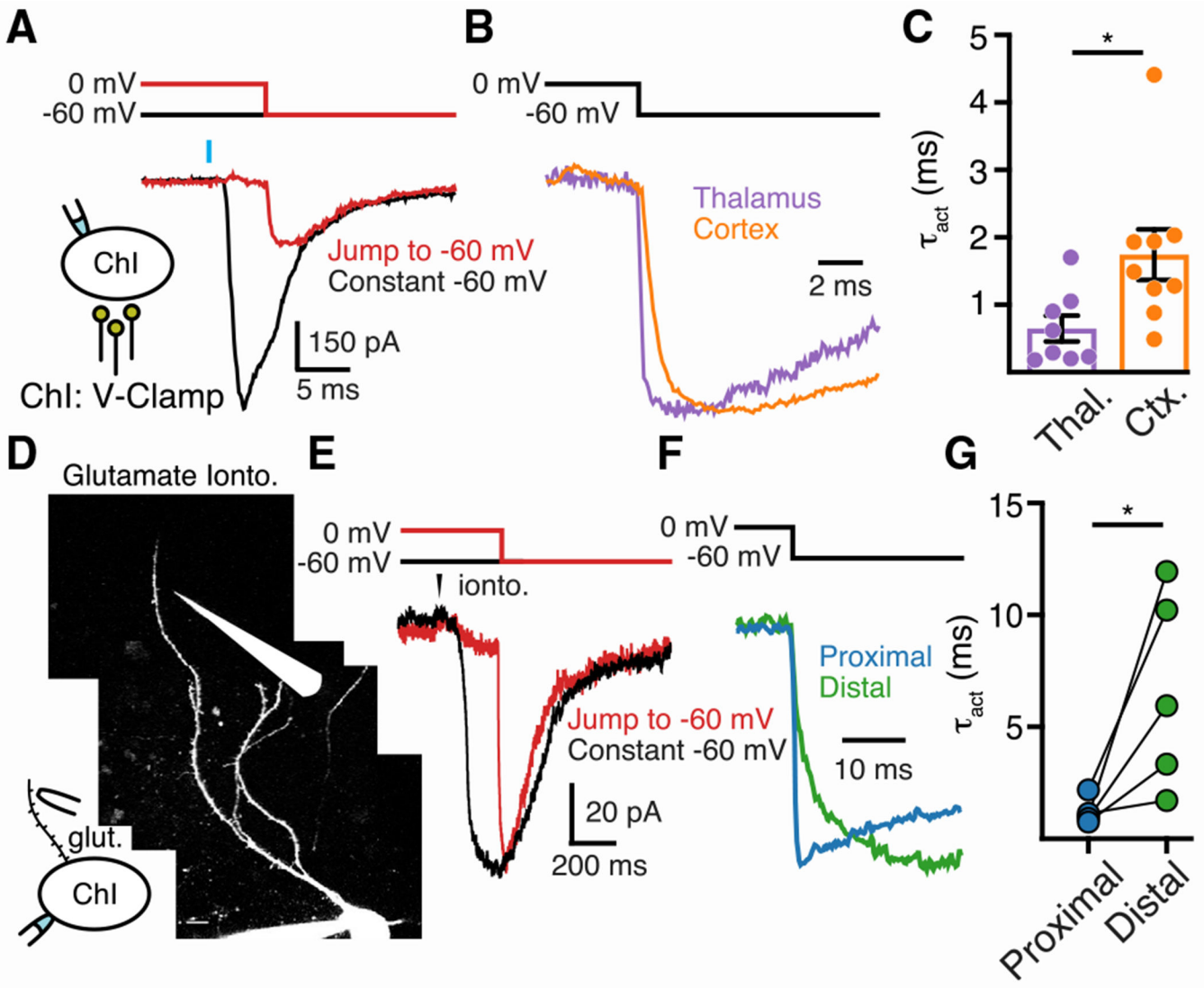

Figure 4. Differential Dendritic Integration of Excitatory Inputs at ChI Synapses

(A) Example trace illustrating voltage-jump protocol. The black trace represents an optogenetically evoked EPSC continually recorded at V_h = −60 mV (single pulse, 2 ms, 470 nm). The red trace represents an EPSC in the same cell recorded at 0 mV and then at −60 mV, 5 ms following the same light stimulation. At 0 mV, although channels are open following glutamate release, there is no driving force. When the voltage is stepped to −60 mV, driving force is initiated, and the current activates over a time that is related to the capacitance between the channels activated and the cell body.

(B) Averaged traces showing slower activation of cortically evoked EPSCs (n = 9) versus thalamically evoked EPSCs (n = 8) (single pulse, 2 ms, 470 nm).

(C) Quantification of slower τ of activation (τ_{act}) of cortically evoked (n = 9) versus thalamically evoked (n = 8) EPSCs recorded in voltage-jump protocol ($p < 0.05$, Mann-Whitney). Error bars indicate ± SEM.

(D) Representative 2-photon microscopy image of a filled ChI (Alexa 594). An iontophoretic pipette with glutamate is positioned opposed to a distal section of the ChI dendrite. Scale bar 10 μm.

(E) Example trace illustrating iontophoresis during voltage-jump protocol. The black trace represents an excitatory current, evoked via iontophoresis of glutamate, continually recorded at V_h = −60 mV. The red trace represents an iontophoresis-evoked current in the same cell recorded at V_h = 0 mV and moved to V_h = −60 mV 250 ms.

(F) Representative traces showing slower activation of iontophoretic currents evoked at distal dendritic locations versus proximal locations.

(G) Quantification of slower τ_{act} of distally evoked versus proximally evoked iontophoretic currents recorded in voltage-jump protocol (n = 5; $p < 0.05$, Student's paired t test).

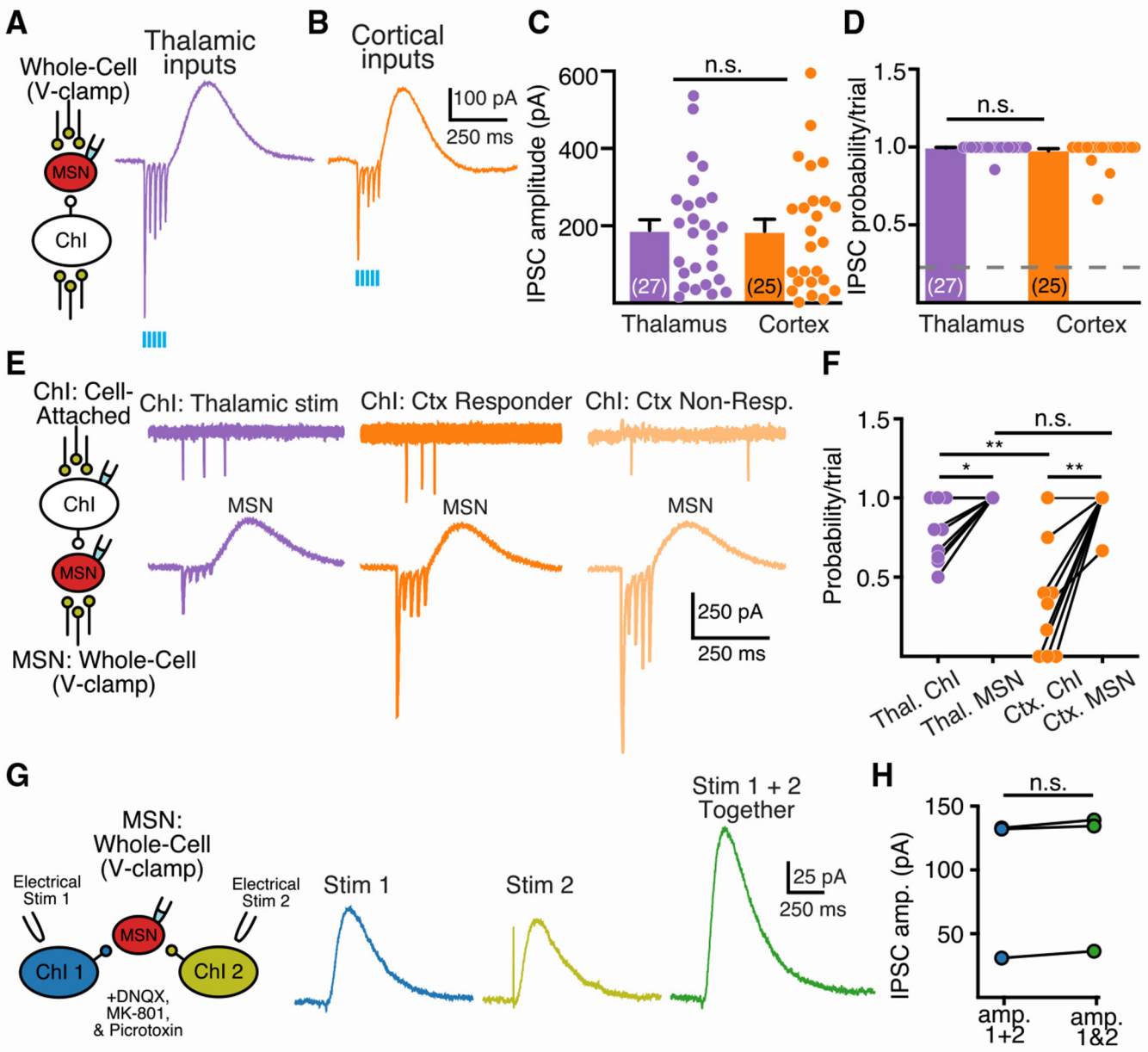

Figure 5. Differential ChI Response to Excitatory Stimuli Evokes Similar Ach Release onto MSNs

(A) Representative voltage clamp recording of an MSN overexpressing GIRK2 channels. Thalamic stimulation (5 pulses, 50 Hz, 470 nm) evokes AMPA EPSCs in MSNs, followed by an M4-muscarinic receptor-mediated IPSC resulting from ChI firing.

(B) Representative trace from a GIRK2-expressing MSN, displaying that cortical stimulation evokes similar levels of ACh release to thalamic stimulation.

(C) Distribution of M4-IPSC amplitudes showing no difference in ACh release evoked between thalamic (n = 27) and cortical (n = 25) stimuli ($p > 0.05$, Mann-Whitney). Error bars indicate ± SEM.

(D) Distribution of IPSC probabilities following the stimulus for each input. The dashed line represents the baseline IPSC probability during the 5 s preceding the stimulus (mean

probability for each 250-ms stimulus bin + 2 standard deviations). The probability of thalamically evoked (n = 27) and cortically evoked (n = 25) IPSCs did not differ (n > 0.05, Mann-Whitney). Error bars indicate± SEM.

(E) Representative dual paired recordings of ChIs (current clamp) and MSNs (voltage clamp, V_h = −60 mV) illustrating consistent M4-IPSCs despite differing ChI firing probabilities.

(F) Paired quantification of ChI AP probability and MSN M4-IPSC probability during dual paired recordings described in (E) (n = 9 for both groups; Wilcoxon matched pair signed rank). * p < 0.05, ** p < 0.01.

(G) Representative traces illustrating the arithmetic summation (stim 1 + 2) of M4-IPSCs evoked via two separate minimal electrical stimuli, approximately 500 μm apart (stim1 and stim 2).

(H) Distribution of summed amplitudes (stim 1 amplitude + stim 2 amplitude) and amplitudes of simultaneous stimulation (stim 1 and 2 amplitudes) (n = 3; p > 0.05, Student's paired t test).

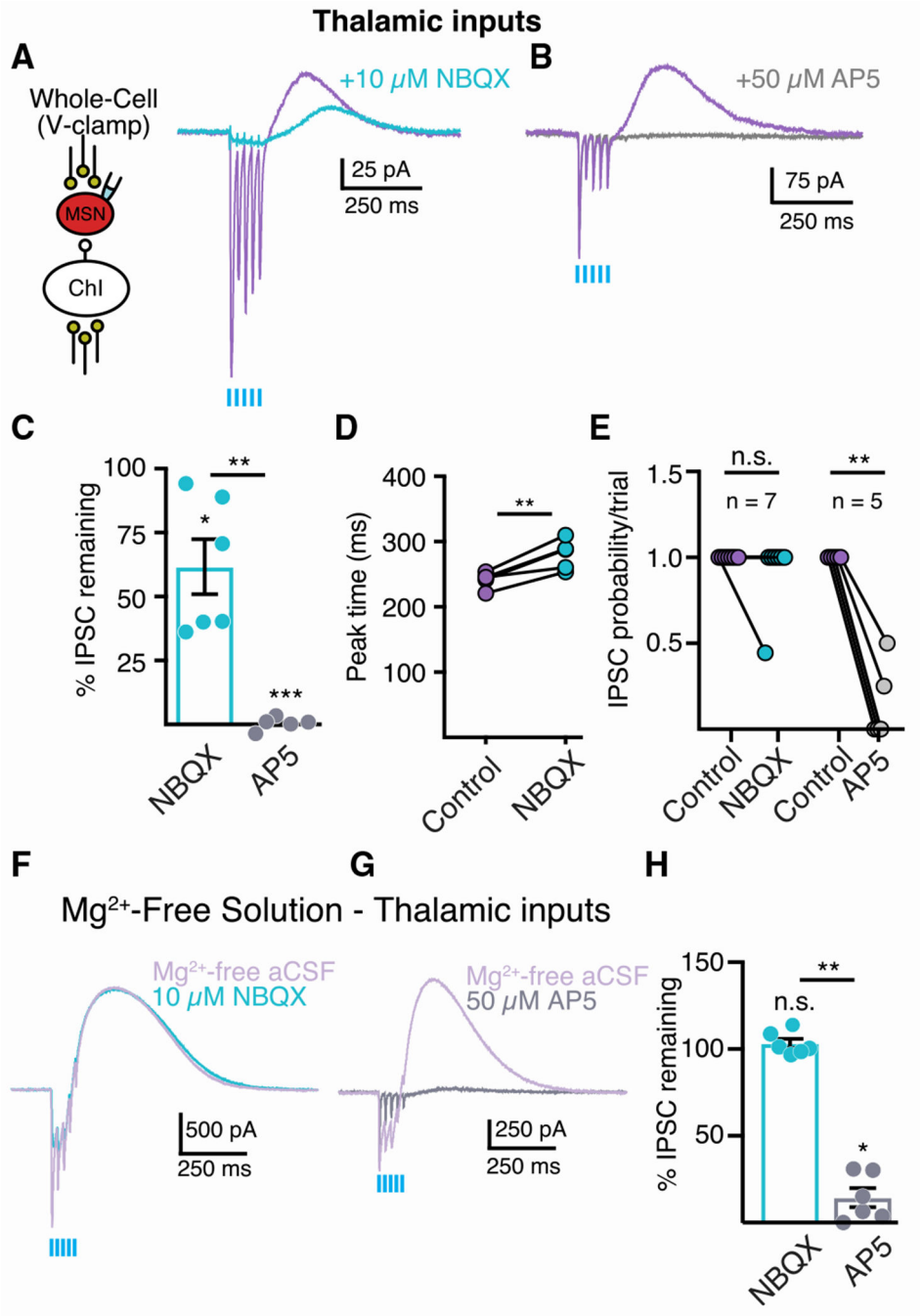

Figure 6. NMDA Receptors Are Critical for Thalamically Evoked Ach Release

(A) Representative trace showing inhibition of thalamically evoked M4-IPSCs in the presence of NBQX (10 μM).

(B) Representative trace showing complete inhibition of thalamically evoked M4-IPSCs in the presence of AP5 (50 μM).

(C) Quantification of M4-IPSC inhibition due to glutamatergic antagonists indicates stronger role for NMDA receptors in thalamically evoked Ach release (NBQX: n = 7, AP5: n = 5). *p < 0.05, **p < 0.01, ***p < 0.001. Error bars indicate ± SEM.

(D) Longer thalamically evoked M4-IPSC peak time in the presence of NBQX (10 μM) (n = 7, $p < 0.01$, Wilcoxon matched pair signed rank). **$p < 0.01$. Error bars indicate ± SEM.
(E) Distribution of IPSC probability shows consistent thalamically evoked Ach release during AMPA receptor antagonism but frequent failure when antagonizing NMDA receptors (NBQX: n = 7, $p > 0.05$; AP5: n = 5, $p < 0.01$; Wilcoxon matched pair signed rank).
(F) Representative trace showing no inhibition of thalamically evoked M4-IPSCs in Mg^{2+}-free artificial cerebrospinal fluid (aCSF) during bath application of NBQX (10 μM).
(G) Representative trace showing complete inhibition of thalamically evoked M4-IPSCs in Mg^{2+}-free aCSF during bath application of AP5 (50 μM).
(H) Quantification of M4-IPSC inhibition due to glutamatergic antagonists in Mg^{2+}-free aCSF indicates stronger role for NMDA receptors in thalamically evoked ACh release (n = 6 for all groups). *$p < 0.05$, **$p < 0.01$. Error bars indicate ± SEM.

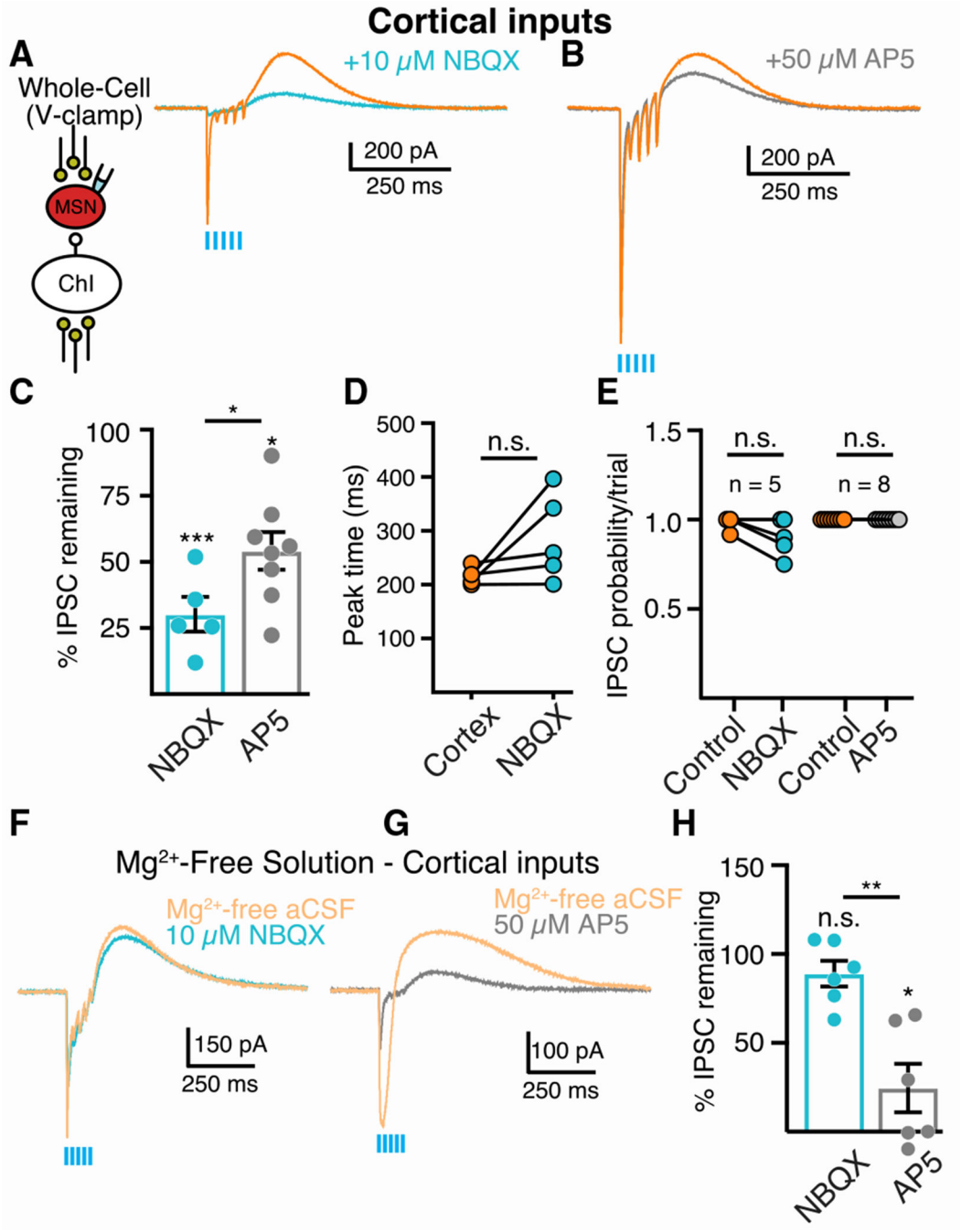

Figure 7. Cortically Evoked ACh Release Relies on Both AMPA and NMDA Receptors

(A) Representative trace showing inhibition of cortically evoked M4-IPSCs in the presence of NBQX (10 μM).

(B) Representative trace showing complete inhibition of cortically evoked M4-IPSCs in the presence of AP5 (50 μM).

(C) Quantification of M4-IPSC inhibition due to glutamatergic antagonists indicates stronger role for AMPA receptors in cortically evoked ACh release (NBQX: n = 5; AP5: n = 8). *p < 0.05, **p < 0.01, ***p < 0.001. Error bars indicate ± SEM.

(D) No difference in cortically evoked M4-IPSC peak time in the presence of NBQX (10 μM) (n = 5, $p > 0.05$, Wilcoxon matched pair signed rank). Error bars indicate ± SEM.
(E) Distribution of IPSC probability shows consistent cortically evoked Ach release under all conditions (NBQX: n = 5, $p > 0.05$; AP5: n = 8, $p > 0.05$; Wilcoxon matched pair signed rank).
(F) Representative trace showing slight inhibition of cortically evoked M4-IPSCs in Mg^{2+}-free aCSF during bath application of NBQX (10 μM).
(G) Representative trace showing strong inhibition of cortically evoked M4-IPSCs in Mg^{2+}-free aCSF during bath application of AP5 (50 μM).
(H) Quantification of M4-IPSC inhibition due to glutamatergic antagonists in Mg^{2+}-free aCSF indicates stronger role for NMDA receptors in cortically evoked ACh release under this condition (n = 6 for all groups). *$p < 0.05$, **$p < 0.01$. Error bars indicate ± SEM.

KEY RESOURCES TABLE

REAGENT or RESOURCE	SOURCE	IDENTIFIER
Bacterial and Virus Strains		
AAV9.hSynapsin.tdTomato.T2A.mGIRK2-1-A22a.WPRE.bGH	University of Pennsylvania Viral Core	V3992MI-R
AAV5.EF1a.DIO.hChR2(H134R)-eYFP.WPRE.hGH	University of Pennsylvania Viral Core	AV-5-20298P
AAV9.SynP.DIO.tdTomato.T2A.mGIRK2-1-A22A.WPRE.bGH	University of Pennsylvania Viral Core	V5688R
AAV5.EF1a.DIO.mCherry	UNC Viral Core	AV4311E
Chemicals, Peptides, and Recombinant Proteins		
D-AP5	Tocris	Cat # 0106
NBQX	Tocris	Cat # 0373
Picrotoxin	Tocris	Cat # 1128
Scopolamine hydrobromide	Tocris	Cat # 1414
QX 314 chloride	Tocris	Cat # 2313
Glutamate	Sigma Aldrich	56-86-0
Experimental Models: Organisms/Strains		
C57BL/6J	Jackson Labs	Stock # 000664
Tg(Adora2a-cre)KG139Gsat	MMRRC	Stock #036158
B6;Cg-Tg(Camk2a-cre)T29-1Stl/J	Jackson Labs	Stock # 005359
B6;129S6-Chat$^{tim2(cre)Lowl}$/J	Jackson Labs	Stock # 006410
Software and Algorithms		
Axograph X	Axograph Scientific	https://axograph.com
MATLAB_R2017b	MathWorks	https://www.mathworks.com
Prism 7	Graphpad	https://www.graphpad.com
Toronado	Custom Software from Dr. Ben Strowbridge	N/A